4 Nuclear Explosions and their Environmental Contamination

YU. A. IZRAEL, E. D. STUKIN, V. N. PETROV, L. ANSPAUGH, A. DOURY, R. J. C. KIRCHMANN AND E. VAN DER STRICHT

4.1 FORMATION AND FRACTIONATION OF RADIONUCLIDES

4.1.1 General characteristics of radionuclides and processes after a nuclear explosion

Most of the contamination from nuclear explosions has resulted from detonations in the atmosphere, especially those near or on the Earth's surface, and from underground detonations that were designed to produce craters.

In order to predict and analyse the atmosphere and terrestrial radioactive contamination it is necessary to know in detail:

1. the nature of the source (size and shape of the radioactive cloud, processes within the cloud, distribution of radioactive particles by size, and distribution of the radionuclides within and on the particles);
2. the meteorological situation (wind velocity with height and precipitation);
3. the distribution of radionuclides on the ground (fallout pattern);
4. the prevalence of foodchains and the intake of contaminated food by animals and humans.

These factors, with additional detail, are indicated in Figure 4.1.

The first two factors determine the character of the atmospheric transport of the debris, the formation of fallout and the principal radiation characteristics, i.e. the external gamma-exposure rate and the radionuclide composition of fallout. These subjects are considered in detail in Izrael (1996).

An atmospheric nuclear explosion produces a radioactive cloud, which depending on the explosive yield, rises to an altitude from several to several tens of kilometres.

A cratering explosion produces a cloud (which rises up to an altitude of several kilometres) and a base surge, which has a height of about 20–25% of the main cloud.

Nuclear Test Explosions: Environmental and Human Impacts
Edited by Sir F. Warner and R. J. C. Kirchmann

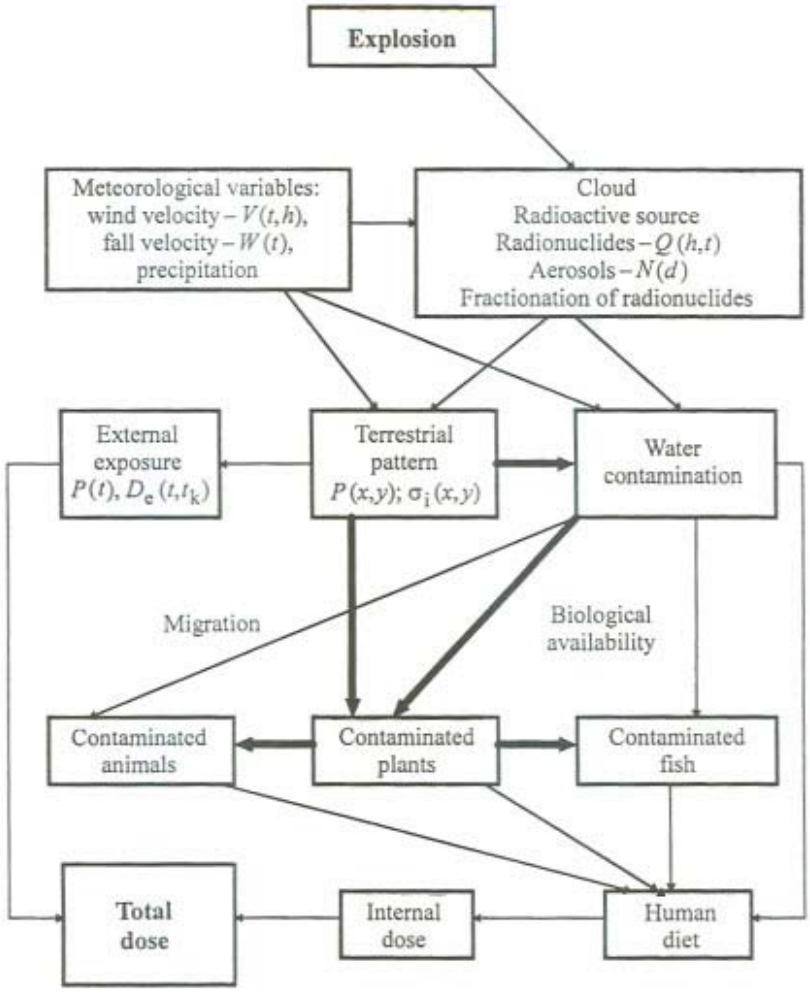

Figure 4.1 The scheme of transformation and transport pathways of radionuclides from nuclear explosions and the consequent atmospheric and terrestrial radioactive contamination.

Radioactive debris consists primarily of fission products and neutron-activation products, both of which may be mixed with a substantial amount of soil and material from the supporting tower and explosion device.

During the first tens of seconds of fireball and cloud formation very important processes occur in the condensation of vaporized products on the particulate matter that may be present. These processes determine the distribution of various radionuclides relative to the size of particles; radionuclides with high

melting points tend to be distributed throughout the volume of larger particles, whereas volatile radionuclides tend to be confined to the surface of particles. As small particles contain most of the total surface area available, volatile radionuclides tend to be associated with smaller particles. Later, particles are transported to various distances depending upon their size, among other factors. Thus, the processes that occur during the first tens of seconds play a decisive role in the radionuclide composition of the contamination as a function of distance from the explosion.

4.1.2 Formation of aerosol particle-carriers of radioactivity

A subsurface nuclear explosion ejects into the atmosphere around 5000 t of soil per explosion yield of 1 kt; 180–200 t of this amount is melted, and 1.5 to 25 t kt^{-1} is vaporized (in the case of an underground explosion up to 50–70 t kt^{-1} is vaporized).

In the case of ground-surface explosions less soil (or water, if exploded over water) is ejected into the fireball and the cloud; in the case of atmospheric explosions the cloud may contain essentially only the matter of the device itself. In the latter case, spherical radioactive particles of several micrometres diameter are formed only as a result of the condensation of the material, whereas in the ground (surface) and underground (cratering) explosions, radioactive particles are produced as a result of the fusing of radioactive material with entrained soil.

Two principal types of particles are formed: spherical (or drop-form) particles formed, as a rule, by fusion of silicate material (for example, volcanic rock, obsidian, etc.), which are up to 1–2 mm in size, and angular particles of irregular forms that have not been fused. In addition there are combinations of the two forms.

Radionuclides in spherical particles are distributed either throughout the entire volume, or through a thick layer of the volume. The radionuclides associated with angular, irregular particles are, as a rule, attached to the surface. A substantial amount of experimental data on radioactive particles and their radionuclide composition has been published (Klement, 1964; Izrael *et al.*, 1970a; Izrael, 1973).

The total particle-activity and size distribution for a surface (and underground) explosion (and for the Chernobyl accident) can be expressed by a lognormal law, i.e. activity fraction $A(d_1, d_2)$ connected with particles with diameter from d_1 to d_2 is equal to

$$A(d_1, d_2) = \frac{1}{\sigma\sqrt{2\pi}} \int_{\lg d_1}^{\lg d_2} \exp\left[-\frac{(\lg d - \lg \bar{d})^2}{2\sigma^2}\right] d(\lg d) \qquad (4.1)$$

where d is the particle diameter, $\bar{d}$ and σ are distribution parameters.

The above distribution is not strongly related to explosion yield, but it does depend substantially on the soil type. For example, for Nevada soil lg $\bar{d}$ = 2.053 and σ = 0.732, for coral soil lg $\bar{d}$ = 2.209 and σ = 0.424 (Stewart, 1956).

Models that describe the movement of radioactive particle distribution in the atmosphere often uses particle fall velocity distributions $N(W)$. For example:

$$N(W) = \frac{a^{n+1}}{\Gamma(n+1)} W^n e^{-aW} \tag{4.2}$$

where W is the particle fall velocity, Γ is the gamma-function, and a, n are distribution parameters. In one particular case studied by Petrov and Pressman (1962) it was found that $n = 2$ and $a = 0.06$.

Vaporized explosion debris transforms into melted (fused) soil particles in accordance with thermodynamic conditions in the fireball as well as with the physical and chemical characteristics of the elements. Soil particles solidify very quickly in the fireball; for example, in about 7 s, in an explosion yield of 20 kt and in about 40 s for an explosion yield of 1 Mt.

4.1.3 Fractionation of radionuclides

The physical and chemical form (i.e. gaseous, intermediate, or refractory) of the radionuclides in a fission-product mass chain during fireball formation is very important in determining the association of radionuclide activity with particle size. Several of the more important mass chains are shown in Table 4.1. It can be seen in Table 4.1 that in the first tens of seconds after the explosion, precursors of ^{89}Sr, ^{90}Sr and ^{137}Cs are in the form of noble gases, ^{89}Kr, ^{90}Kr and ^{137}Xe; therefore the product radionuclides (e.g ^{89}Sr, ^{90}Sr and ^{137}Cs) are not found within the particles that condense during the early post-detonation phases. Rather, ^{89}Sr, ^{90}Sr and ^{137}Cs attach to particles according to the surface area available at the later times when they condense. In contrast, radionuclides such as ^{95}Zr and ^{144}Ce are already in the form of refractory elements within the first seconds and thus are found distributed throughout the volume of particles that condense during the early phases. A value, F_i can be calculated (Izrael, 1973):

$$F_i = \frac{Q_i^{\mathrm{V}}(t)}{Q_i(t)} \tag{4.3}$$

i.e. the relation between the stage the ith chain radionuclide reached by the moment t inside the melted particle $Q_i^{\mathrm{V}}(t)$ and the total amount of radionuclides in the given chain $Q_i(t)$.

The dependence of the total activity, $A(r)$, of the individual radioactive particles on their radius, r, is subject to the power law $A(r) = k \times r^n$, where k is

Table 4.1 Mass chains of certain fission products.

Mass chain	Volatile	Intermediate	Refractory
89	4.4 s* $^{89}Br_{35}$ → (48.2)** → 3.2 min $^{89}Kr_{36}$ (40.7)	→13.4 min $^{89}Rb_{37}$ → (4.1)	50.5 day $^{89}Sr_{38}$ → (0.05) → stable $^{89}Y_{39}$
90	1.6 s $^{90}Br_{35}$ → (27.5) → 33 s $^{90}Kr_{36}$ (56.7)	→ 2.7 min $^{90}Rb_{37}$ → (13.9)	28 yr $^{90}Sr_{38}$ → (0.41) 64 h $^{90}Y_{39}$ → stable $^{90}Zr_{40}$
95	short $^{95}Kr_{36}$ (0.1)	→ 2 s $^{95}Rb_{37}$ → (7.2)	40 s $^{95}Sr_{38}$ → (49.1) → 10 min $^{95}Y_{39}$ → (39.7) → 65 day $^{95}Zr_{40}$ → (3.8) → 35 day $^{95}Nb_{41}$ → → stable $^{95}Mo_{42}$
137	24.4 s $^{137}I_{53}$ → (54.2) → 3.9 min $^{137}Xe_{54}$ (32.5)	→ 30 y $^{137}Cs_{55}$ (2.32)	0.95 → 2.6 min $^{137m}Ba_{56}$ ↓ 0.05 → stable $^{137}Ba_{56}$
144	short $^{144}Xe_{54}$ (0.2)	→ 1.5 s $^{144}Cs_{55}$ → (2.7)	3.5 s $^{144}Ba_{56}$ → (49.1) → 15 s $^{144}La_{57}$ → (39.7) → 290 day $^{144}Ce_{58}$ → (3.8) → 17 min $^{144}Pr_{59}$ → → stable $^{144}Nd_{60}$

* Half-life.
** % (Izrael, 1996).

a parameter to be fitted and $2.0 < n < 3.0$, i.e. at $n = 2.0$ contamination is only on the surface of the particle and at $n = 3.0$ contamination is spread throughout the volume of the particle (Figure 4.2).

Thus, the physical processes that occur within the fireballs and which result in different radionuclides being attached to particles of different size, result in the 'fractionation' of radionuclides. Radionuclides that condense at later times attach themselves to particles according to the surface area available, which is always associated with smaller particles. Such smaller particles typically remain airborne for longer times than do the larger particles with the refractory elements distributed throughout their volume.

Radionuclide fractionation can be considered as a deviation of the radionuclide ratio (in particles, zones of radioactive fallout, etc.) from the initial

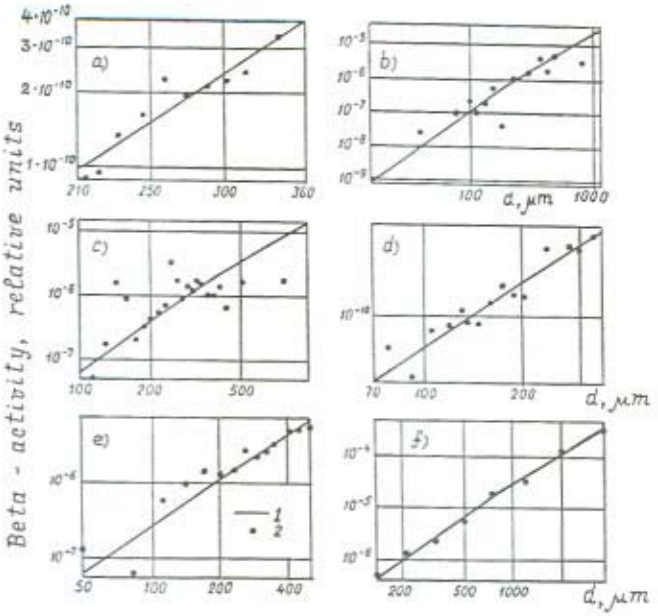

Figure 4.2 Relationship between particle beta-activity and particle size in various experiments: (a) 12 August 1953; (b) 29 July and 5 August 1955; (c) 25 March 1956; (d) 24 August 1956, measurements 3 y after the explosion; (e) 24 August 1956, measurements 3 h after the explosion; (f) 14 September 1961. 1, calculation; 2, experimental data.

ratio at the moment of the explosion. Thus, the fractionation factor of the ith radionuclide to jth radionuclide is

$$f_{i,j}(t,r) = \frac{n_i(t,r)/n_j(t.r)}{[n_i(t)/n_j(t)]_T} \tag{4.4}$$

where the index T denotes the theoretical ratio of these radionuclides (n is the number of nuclei, t is the time and r is the radius of the particles).

Fractionation factors are important characteristics of atmospheric and terrestrial contamination. They change significantly for different particles and different zones of contamination, even for the same explosion (up to 100 times). To characterize fractionation in a fallout pattern from a given explosion (or for an explosion as a whole) one can construct correlation plots of logarithms of fractionation factors. It is common to make reference to two radionuclides of opposite (by volatility) properties of elements (mass chains); usually these are ^{89}Sr and ^{95}Zr.

Figure 4.3 shows examples of correlation plots for different radionuclides produced by the USSR crater forming explosion named Sary-Uzen, and the

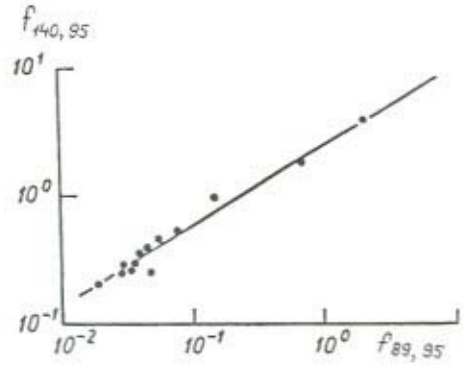

Figure 4.3 Correlation plots of fractionation factors for various radionuclides in the fallout pattern from USSR crater explosion shaft '1003'.

drilled shaft '1003' (Izrael *et al.*, 1970a; Izrael, 1973). A similar correlation plot is shown in Figure 4.4 for an atmospheric explosion (Freiling, 1961).

It follows from the plots that

$$\lg f_{i,89} = a_i + b_i \lg f_{95,89} \tag{4.5}$$

where a_i is the value of the 'cut-off' (ordinate) and $b_i = \operatorname{tg} \alpha$ is the slope of the regression line. Values of a_i and b_i depend on the choice of radionuclide k as the reference.

It can be shown (Freiling, 1963) that $b_i = n_{i-2}$ and

$$a_i = \frac{b_i(1 - b_i)\sigma^2}{4,6} \neq 1 \tag{4.6}$$

Here, σ^2 is the dispersion in the lognormal distribution of a particle activity and mass by sizes $2 \leq n_i \leq 3$ is the power index of particle size distribution of activity.

It turned out that

$$\lg f_{i,89} = \sqrt{F_i} \lg f_{95,89} \tag{4.7}$$

where F_i is determined from equation (4.3) (Figure 4.5).

It is of interest to note that value of v_i is not related to the fission type (unlike the value of the 'cut-off' variable a_i). Values of a_i and b_i depend on the choice of radionuclide, k, as a reference.

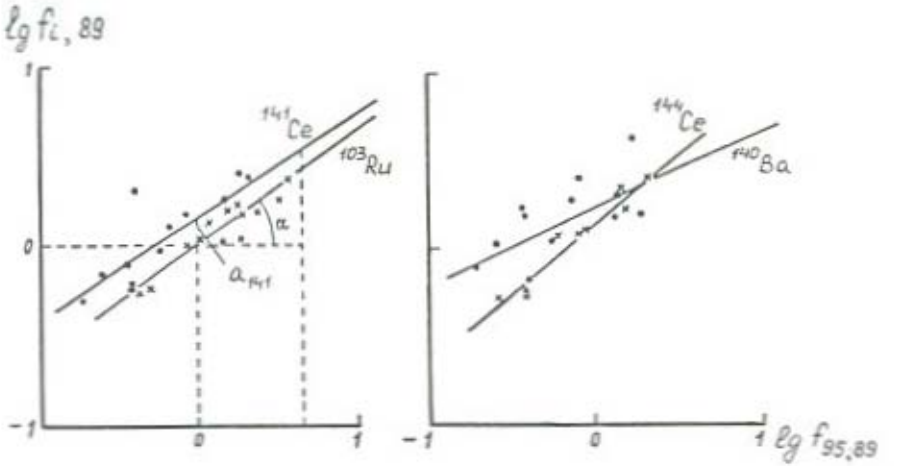

Figure 4.4 Illustrative correlation plot of fractionation factors for an atmospheric nuclear explosion.

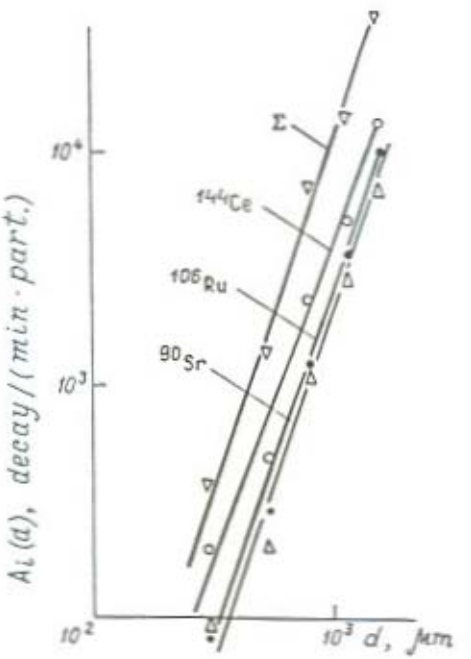

Figure 4.5 Size dependence of various radionuclides activity in particles within the first few seconds of an explosion (data obtained from USSR crater explosion shaft '1003').

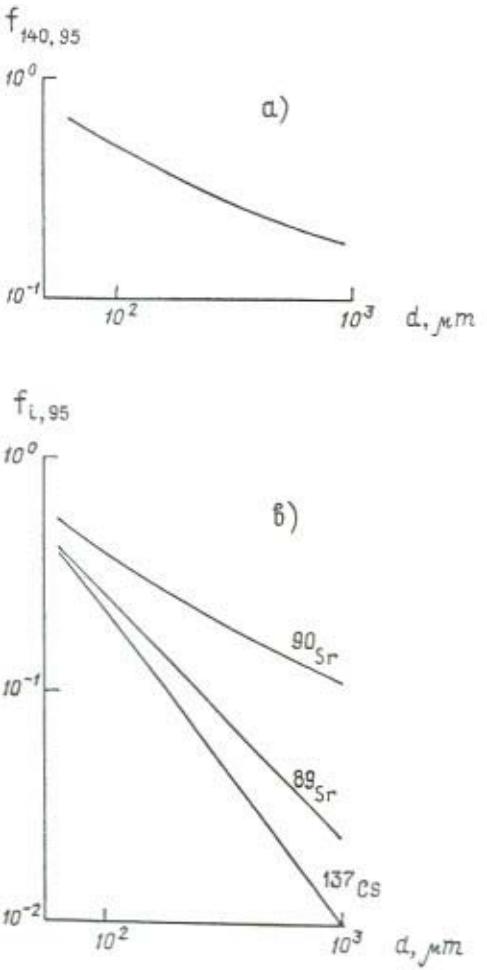

Figure 4.6 The relationship between fractionation factors and particle size for ^{140}Ba (a), ^{89}Sr, ^{90}Sr and ^{137}Cs (b).

Having assumed the respective models of particle activity (distribution with particle size) on the surface of a particle and in the structure of a particle theoretical relationships can be constructed (Izrael, 1973) between fractionation factors for various radionuclides and particle size (Figure 4.6). The application of these models has made it possible to calculate the fraction and distribution of radionuclides deposited within the immediate vicinity of explosions of various yields. The validation of these results with independent material is shown in Figure 4.7. Here we see a correlation plot of calculated values with those

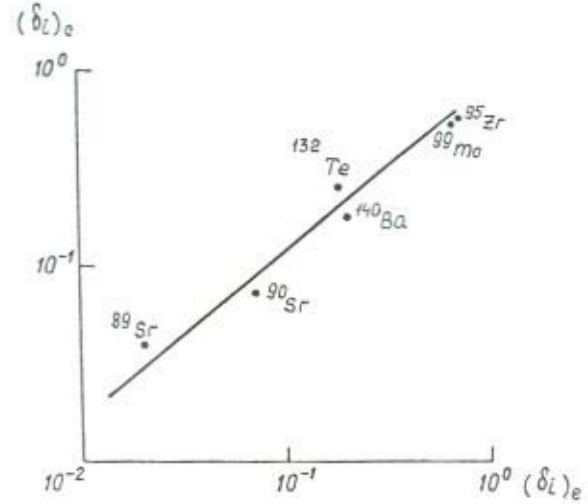

Figure 4.7 Correlation plot of calculated $(\delta_i)_c$ and experimental $(\delta_i)_e$ fractions of radionuclides deposited from fallout in the immediate vicinity of a low-yield ground explosion.

obtained experimentally from fallout in the immediate vicinity of a small explosion (Small-boy) carried out in the USA. These data demonstrate that the experimental and calculated values coincide.

Table 4.2 lists experimentally obtained integral values of lg α_i for fallout patterns from atmospheric and ground-surface explosions (Freiling, 1963).

Further, if one considers fractionation factors at different distances from ground zero their dependence on distance is obvious. Figure 4.8 shows the dependence of fractionation factors (integrated across the pattern) on the distance x/Hu from the ground zero for four crater nuclear explosions in the former USSR (Izrael *et al.*, 1970a). For the normalized distance, x is the distance along the pattern axis, u is the wind speed, and H is the cloud height. A distinct relationship between fractionation factors and distance is observed in this figure.

Table 4.2 Values for lg α_i when correlating various radionuclides from atmospheric nuclear explosions.

Radionuclide	lg α_i	Radionuclide	lg α_i
^{90}Sr	0.32	^{140}Ba	0.43
^{99}Mo	0.11	^{144}Ce	0.94
^{132}Te	0.60	^{237}U	1.04
^{137}Cs	–0.06	^{239}Np	1.05
^{89}Sr	0	^{95}Zr	1.0

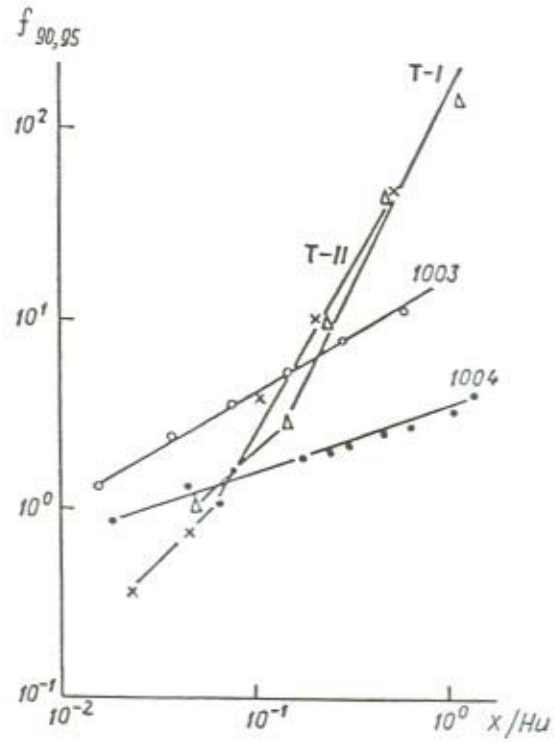

Figure 4.8 Changes of fractionation factors, $f_{90,95}$, with normalized distance x/Hu for various explosions (x, distance along the pattern axis; u, wind speed; H, cloud height).

For radionuclides produced from ground-surface explosions the relative magnitude of fractionation (from 0 to 1 relative to ^{95}Zr, i.e. from 'volatile' to 'refractory') can be presented in the following sequence (Klement, 1964; Izrael, 1973): ^{137}Cs, ^{89}Sr, ^{90}Sr, ^{136}Cs, ^{115}Cd, ^{111}Ag, ^{140}Ba, ^{91}Y, ^{141}Ce, ^{99}Mo, ^{103,106}Ru, radionuclides of rare-earth elements, ^{95}Zr. For underground nuclear explosions this sequence is as follows (Izrael *et al.*, 1970): ^{137}Cs, ^{89}Sr, ^{90}Sr, ^{140}Ba, ^{91}Y, ^{103}Ru, ^{131}I, ^{132}Te, ^{136}Cs, ^{141}Ce, ^{144}Ce, ^{99}Mo, ^{95}Zr. A large amount of experimental data on the radionuclide composition of airborne and fallout material has been published (Klement, 1964).

It is important to note that the established relationships of the dependence of radionuclide fractionation on volatile precursors produced by nuclear explosions does not, naturally, apply to nuclear reactor accidents. In the case of a reactor accident, for example, the behaviour of all caesium isotopes is similar, but the behaviour of strontium isotopes are different (Izrael *et al.*, 1990). In the case of a nuclear reactor accident such as Chernobyl, the caesium and strontium

isotopes behave quite differently, as the volatile precursors of the strontium isotopes have already decayed and strontium itself is not volatile.

4.2 ATMOSPHERIC DISPERSION AND FALLOUT OF RADIONUCLIDES

The spatial pattern of surface radioactivity contamination is formed by the fallout of radioactive particles from the radioactive cloud in passing air masses. One can distinguish a proximal pattern (a few hundred kilometres from ground zero), a remote pattern (formed several days after the explosion) and global fallout occurring over several years, which comprises highly dispersed radioactive particles ejected into the atmosphere and stratosphere.

When describing the pattern one should investigate its spatial pattern (isolines of dose rates or radionuclide deposition density) and determine distinctly the axis of maximum contamination.

4.2.1 Local (proximal) fallout patterns

Patterns from the clouds of high-yield ground and tower-type nuclear explosions are well known (for example, the USA explosions of 1949 on Bikini Atoll and the explosion of 12 August 1953 at the Semipalatinsk Test Site). Figure 4.9 shows spatial distribution of ^{137}Cs contamination density, with the pattern from the explosion of 1953 indicated (Izrael *et al.*, 1994).

It is obvious that spatial distribution patterns will depend much on the size of the cloud and on meteorological conditions, particularly on changes in wind direction at high altitude.

Figure 4.10 shows the relationship between the amount of radioactive products $A(R)$ in various patterns from the explosions of the Semipalatinsk Test Site (Loborev *et al.*, 1994) and the distance R. One characteristic peculiarity of these relationships is that they are power functions:

$$A(R) = A_0 R^{-n} \tag{4.8}$$

Another peculiarity is the occurrence of a conspicuous curve at the beginning of the pattern: it is practically absent in the case of ground explosions, close to ground zero for tower explosions and is variably located depending on the relative height of the explosion for air explosions.

Particularly well studied are patterns of underground cratering explosions (Izrael, 1974). The main characteristics of such explosions carried out in the USA and former USSR are given in Table 4.3. A peculiarity of cratering nuclear explosions is the formation (besides the cloud) of a base surge yield, which results in a circular contamination of the ground zero region (Nordyke

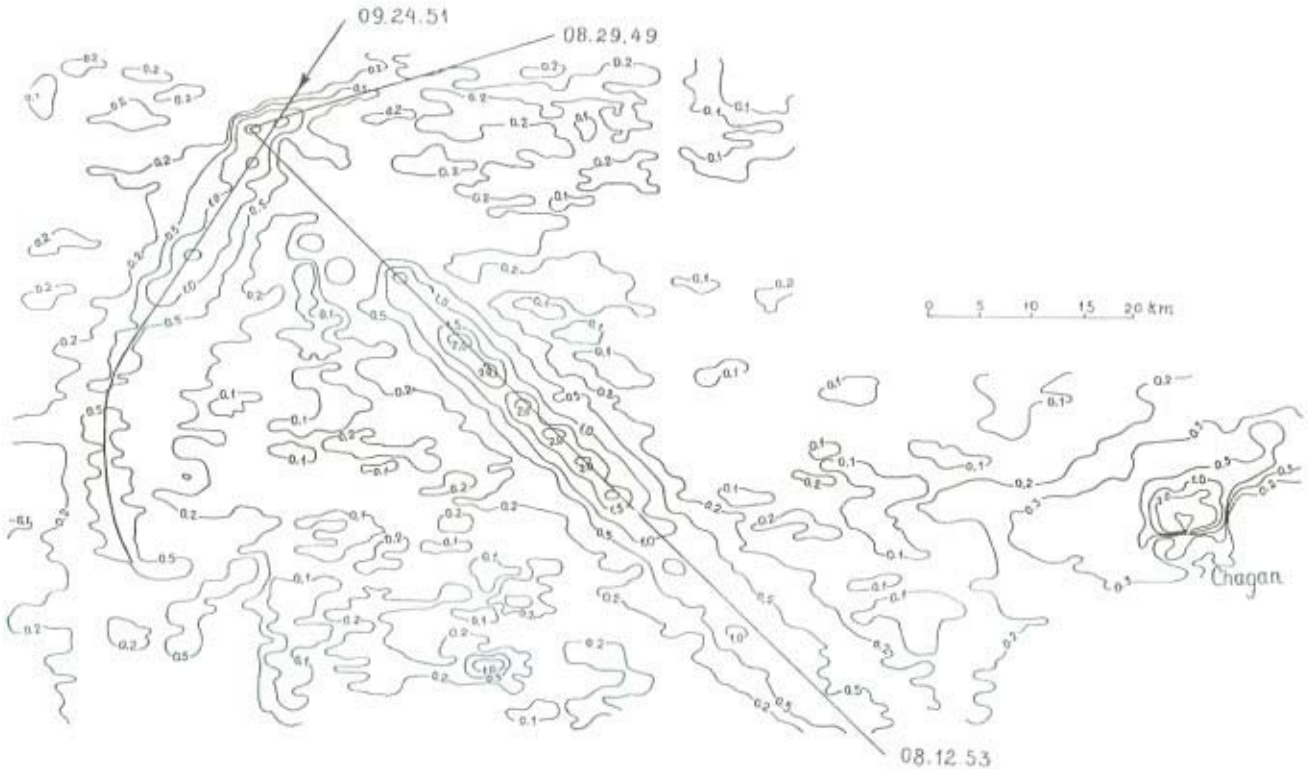

Figure 4.9 The area around the Semipalatisk Test Site contaminated by ^{137}Cs (Ci km^{-2}; multiply by 3.7×10^{10} to obtain becquerels). The survey was undertaken in 1991 (based on Scientific Production Enterprise (SPE) 'Aerogeologia' data). Spatial patterns attributable to individual explosions are shown.

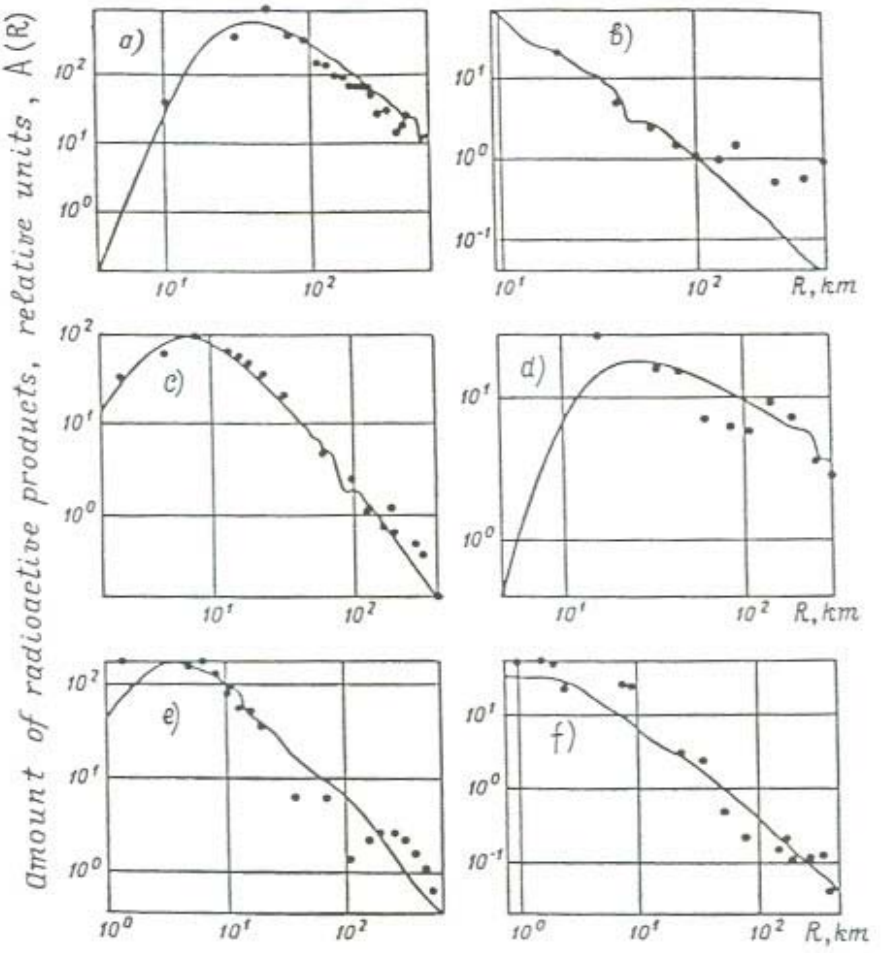

Figure 4.10 Relationship between the amount of radioactive products $A(R)$ in the fallout pattern from the nuclear explosion and distance R from ground zero. Data are for surface nuclear explosions on STS: (a) 12 August 1953; (b) 5 October 1954; (c) 2 August 1955; (d) 24 August 1956; (e) 7 August 1962; (f) 30 October 1962.

and Wray, 1964; Izrael *et al.*, 1970a,b). This contamination, unlike surface contamination, is volumetric in character: i.e. radioactivity is found at depth, down to tens of centimetres and more (Figure 4.11; Izrael *et al.*, 1970b).

Figures 4.12 and 4.13 show the surface pattern of contamination following the underground nuclear explosions '1003' (USSR) (Izrael *et al.*, 1970a) and Sedan (USA) (Klement, 1964). Figure 4.14 shows changes in the dose rate and

Table 4.3 Basic data concerning experimental cratering nuclear explosions*.

Type	Name of the explosion	Country	Yield, kt	Depth, m	$m/kt^{1/3.4}$	Cloud height, m	Amount of material deposited over the pattern***, t	Radioactivity fraction deposited over the pattern, %
Medium yield	'Chagan' ('1004')	USSR	140**	175	41	4800	1400	20
	'Sedan'	USA	104	193	50	3600–4200	1200–1400	4–17
	'Schooner'	USA	30	108	39	4000	340	
Low yield	'Cabriolet'	USA	2.3	52	44.8	120	7	
	'Sary-Uzen' ('1003')	USSR	1.1	48	48	300	35	3.5
	'Danny-Boy'	USA	0.43	33.5	43.2	300	17–30	4–7
Very low yield	'Telkem-1' (T-1)	USSR	0.2	31.4	51	200	0.4	0.2
	'Sulky'	USA	0.092	27.4	56	–	–	–
Row explosion	'Buggy'	USA	1.08 × 5	41.2	41.2	660		
	'Telkem-2' (T-2)	USSR	0.24 × 3	31.4	51	450	1.8	0.3
	'Taiga' ('Canal')	USSR	15 × 3	128				

* All basic data are shown in accordance with official publications (Mikhailov *et al.*, 1996) and (US DOE, 1994).
** Yield on fission is 7 kt in accordance with Mikhailov *et al.* (1996).
*** On power density field.

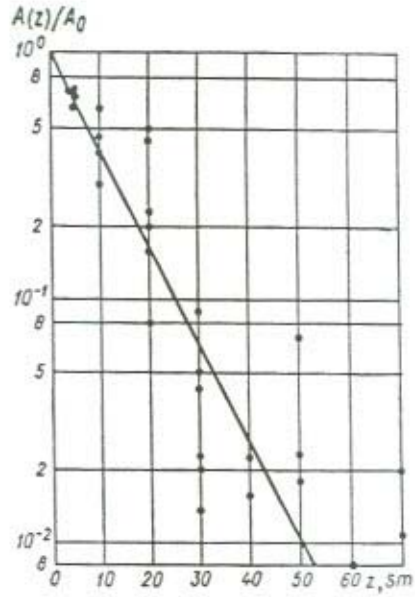

Figure 4.11 The relationship between the specific soil beta-activity and depth in the profile for explosion '1004'.

total amount of radioactive iodine at the ground surface along the plume axis of explosion '1003', and Figure 4.15 shows the relationship between the total amount of ^{131}I and the distance from ground zero for three crater explosions (Izrael *et al.*, 1970b).

4.2.2 Remote pattern (tropospheric fallout)

The remote pattern is characterized by larger spatial scales and much lower contamination densities as compared to the proximal pattern.

Figure 4.16 (Izrael *et al.*, 1995) shows data on the measured activity of radioisotopes ^{95}Zr + ^{95}Nb and ^{103}Ru measured in the USSR after a series of the 1961 high-yield nuclear explosion at the Novaya Zemlya Test Site. In the autumn of 1961, 11 nuclear explosions of more then 1 Mt yield were conducted there, and on 23 and 30 October 1961 two very large devices, with yields of 12.5 and 50 Mt, were exploded (Mikhailov *et al.*, 1996). The explosions were conducted at an altitude of 3.5 and 4 km. The nuclear clouds from all these explosions, having reached a high altitude, spread towards the continental territory of the former USSR (primarily towards the south to southeast). The contamination over a vast area of the former USSR was investigated in April

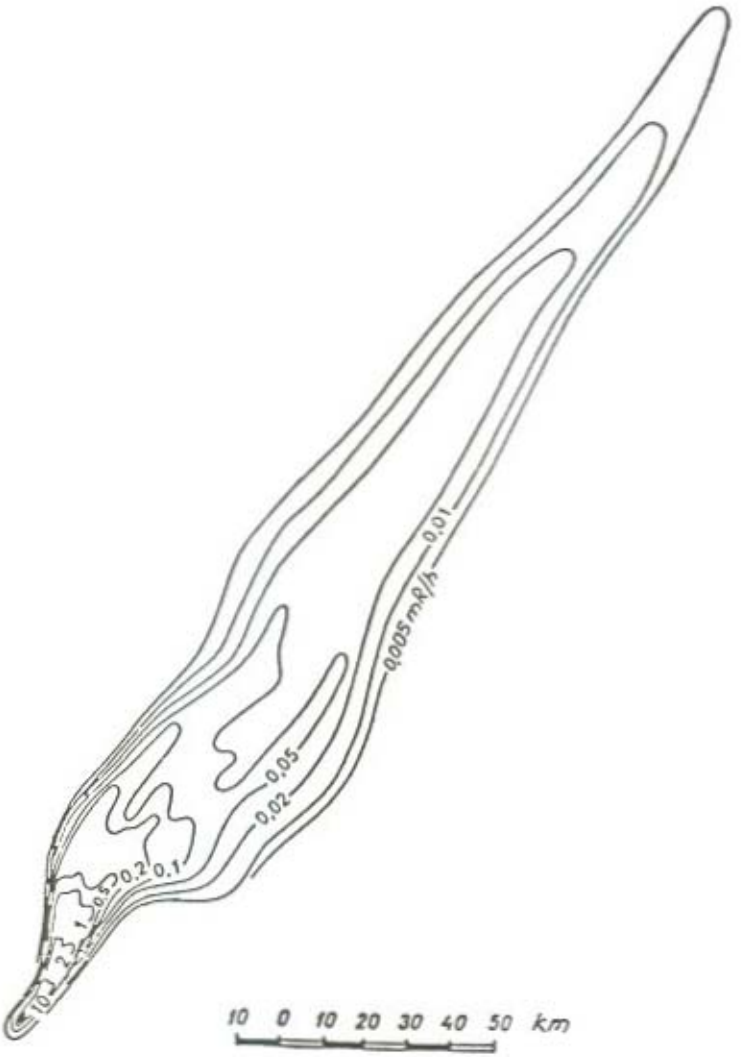

Figure 4.12 Gamma-radiation dose rate distribution in the fallout pattern, one day after explosion '1003'.

1962 by sampling the snow cover present before the nuclear test and which had not melted before sampling.

At least two vast zones of radioactive contamination were found: the first zone in the west of the Ural Mountains (Uralskie Gory), and the second in the Taymyr (Taimyr) peninsula and central Siberia. The maximum surface contamination in April 1962 was: total activity up to 1000 mCi (37 GBq) km^{-2};

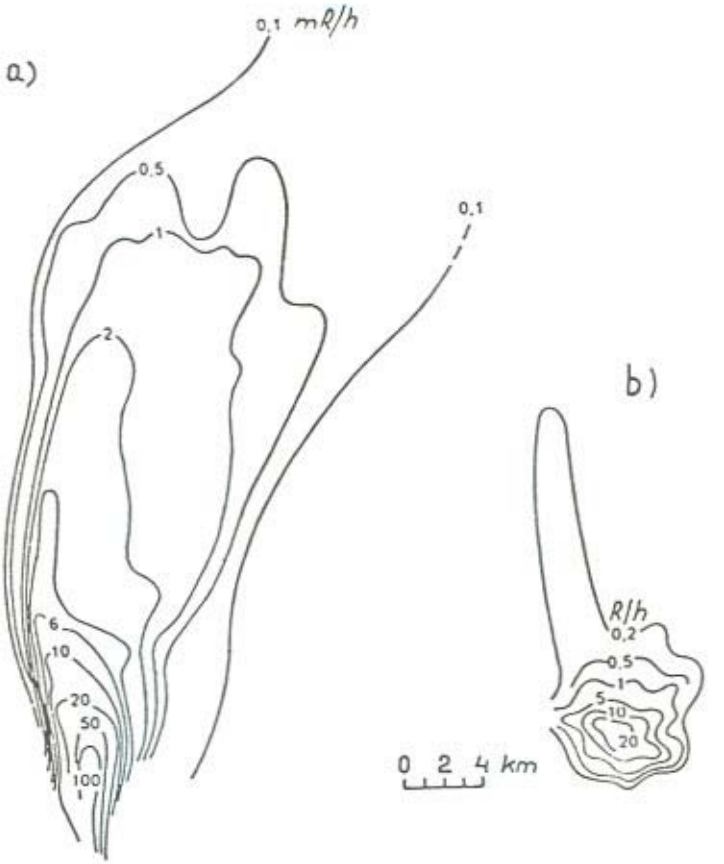

Figure 4.13 Gamma-radiation dose rate distribution in the pattern of fallout contamination (a) and in the pattern of proximal contamination (b) one day after the 'Sedan' explosion.

^{95}Zr + ^{95}Nb up to 300 mCi (11.1 GBq) km^{-2}; ^{103}Ru up to 55 mCi (2.0 GBq) km^{-2}. No noticeable ruthenium isotope fractionation relative to ^{95}Zr was noticed. This contamination corresponds to a maximum external gamma dose radiation of 0.2–0.3 rem (2–3 mSv) between the time the fallout was formed and its complete decay.

In contrast, in the remote fallout from the 'Sedan' crater explosion at a distance of about 1000 km from ground zero, substantial radionuclides fractionation was observed (Table 4.4). It is to be noted that the tritium deposition in the remote fallout from the Chagan crater explosion, shaft '1004' is close to the deposits of other volatile explosion products (Table 4.5).

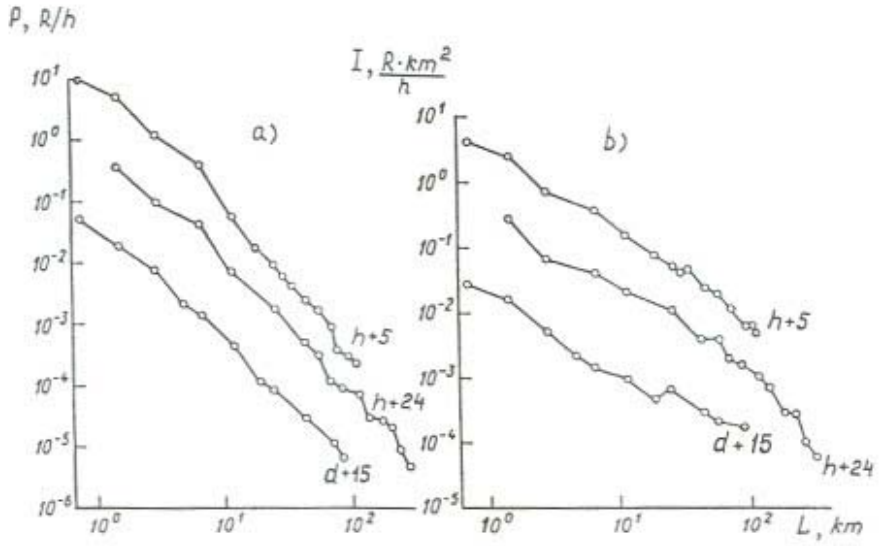

Figure 4.14 Dependence of gamma-radiation dose rates, R/h^{-1} (a) and integral amount of radioactivity, $R\ km^{-2}\ h^{-1}$ (b) on distance *R* along the fallout-contamination axis from explosion '1003'.

A remote pattern of radionuclide fallout was produced by the crater explosion 'Schooner' (USA, NTS, 8 December 1968), as measured over Europe and the USSR.

4.2.3 Global fallout

The products of the very high-yield nuclear explosions reached the higher atmosphere and the lower stratosphere and were transported and deposited globally in a matter of weeks, months and years, mainly in the same latitude belt as the test site.

Figure 4.17 shows the distribution of ^{90}Sr at the Earth's surface in 1963–64 (Klement, 1964). At that time the average deposition density of ^{90}Sr in the Northern Hemisphere (in the band between 70°E and 140°E) was 40 mCi (1.48 GBq) km^{-2}, whereas that of ^{137}Cs was 1.85 times as much. The distribution of ^{137}Cs (contamination density, mCi km^{-2}) of global origin over the territory of the former USSR in the late 1960s is shown in Figure 4.18 (obtained by airborne-gamma survey) (Boltneva *et al.*, 1977).

At first, global fallout included the short-lived radionuclides (^{144}Ce, ^{95}Zr + ^{95}Nb, ^{54}Mn, etc). In total 19.3 MCi (714 PBq) ^{90}Sr, 33 MCi (1.2 EBq) ^{137}Cs

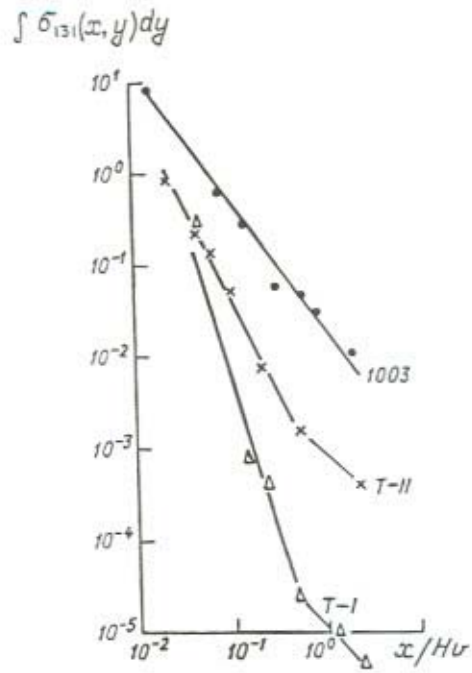

Figure 4.15 The relationship between ^{131}I integral amount and distance along the fallout-contamination axis for three crater explosions.

and up to 1600 MCi (59.2 EBq) of tritium were released into the atmosphere before 1963 (Klement, 1964). It is interesting to note that deposition of ^{137}Cs over central Europe after the Chernobyl nuclear power plant accident is 1.9 MCi (70.3 PBq).

4.2.4 The modelling and prediction of radioactive fallout

Residence times and geographical distribution of the explosion debris and products are determined by the local and global air mass movements and meteorological conditions, as well as by the size and physical properties of the explosion. Any prediction of radioactive contamination deposition requires a detailed knowledge of all processes involved and the physical collection of actual contamination data. This information makes it possible to reconstruct (model) the radioactive contamination source and the various stages of its distribution.

Based on experimental data the contamination source is modelled either as an instantaneous point source (with particles and radioactivity carrier size

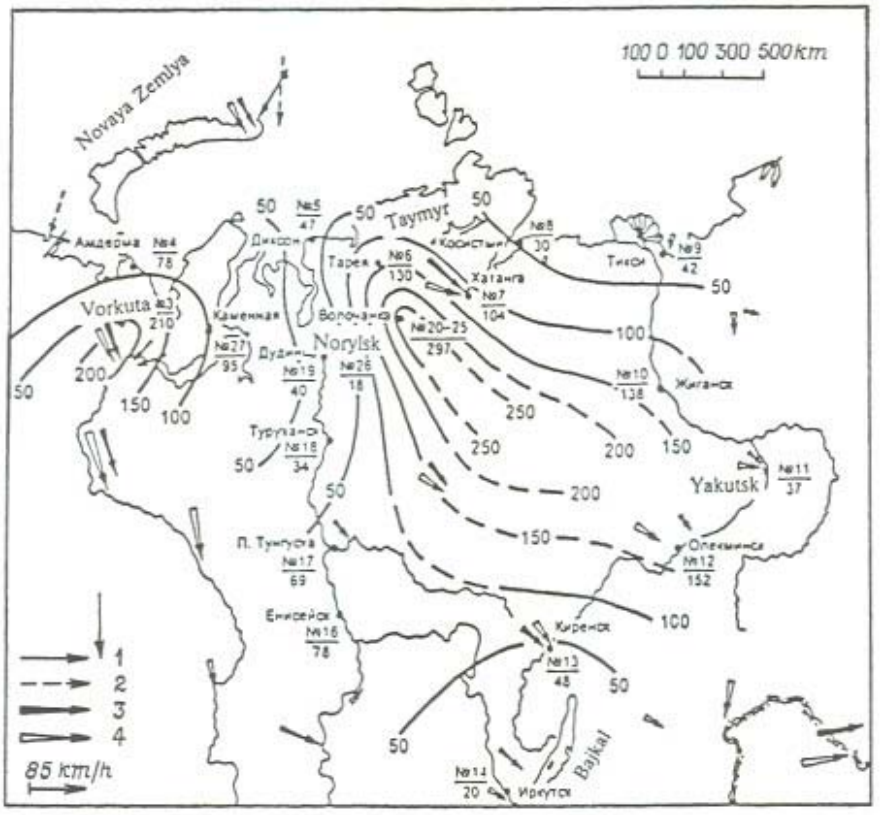

Figure 4.16 A map of the $^{95}Zr + {}^{95}Nb$ deposition pattern based on measurement data of 1962. Sample number (numerator) and terrain contamination density by the end of May 1962 in mCi km^{-2} (denominator) are given near the sampling points. Arrows show mean wind velocity direction at 0–15 km height on 23 (1), 24 (2), 30 (3) and 31 (4) October 1961. To convert mCi to becquerels multiply by 3.7×10^7.

distribution, equations (4.1) and (4.2), for settling velocity)—if there is no wind shift—or as a vertical linear source if there is a windshift. Point-source contamination modelling is the most universal. According to experience gained, however, in most cases modelling of an instantaneous point source is more applicable when developing scenarios for variable contamination patterns.

A model for the fallout prediction from atmospheric plumes emanating from underground explosions has been developed. The basic variable in estimating the fallout pattern in the absence of wind shifts in the atmosphere is settling velocity, W, of the radioactive particles. A simplification of the radioactive particle distribution in the base surge and main cloud is assumed such that at

Table 4.4 Relative content (%) of radionuclides in the remote zone of the 'Sedan' explosion (about 1000 km from ground zero).

Radionuclide	Calculation (Izrael, 1974)	Air filter samples (Krey and Fried, 1965)	Fallout samples (Krey and Fried, 1965)
^{89}Sr	40	43	18
$^{90}Sr + {}^{90}Y$	0.35	0.25	0.2
^{95}Zr	–	0	0
^{91}Y	–	3.4	2.8
^{103}Ru	–	4.0	2.9
^{106}Ru	–	0.9	0.8
^{137}Cs	0.3	0.8	0.45
^{140}Ba	24	24	33
^{140}La	28	24	33
^{141}Ce	–	0	4.9
^{144}Ce	–	0	0.8
^{99}Mo	–	0.4	1.0

Table 4.5 Tritium fallout over the pattern from explosion '1004' (1965).

Distance from ground zero, km	Precipitation collection period	Tritium concentration in precipitation, TR	Tritium deposition, mCi km^{-2}
200	D+2 – D+14 12 days	29 000 ± 1500	945
450	D+1 – D+13 12 days	8400 ± 1200	500
500	D+10 1 day	11 500 ± 1200	90
500*	D+10 1 day	10 500 ± 200	82
500**	D+2 – D+13 11 days	5300 ± 1000	42
500	D+3 – D+10 7 days	3600 ± 1000	60
550	D+6 – D+14 8 days	8800 ± 1250	240
1800	D+5 1 day	12 900 ± 1500	20
3300	D+3 – D+10 7 days	4700 ± 1000	45
550***	Explosion time	2000 ± 1000	14
4000***	Explosion time	1000 ± 1000	10

* Second sample.
** Third sample.
*** Background samples taken outside the pattern (area of contamination).

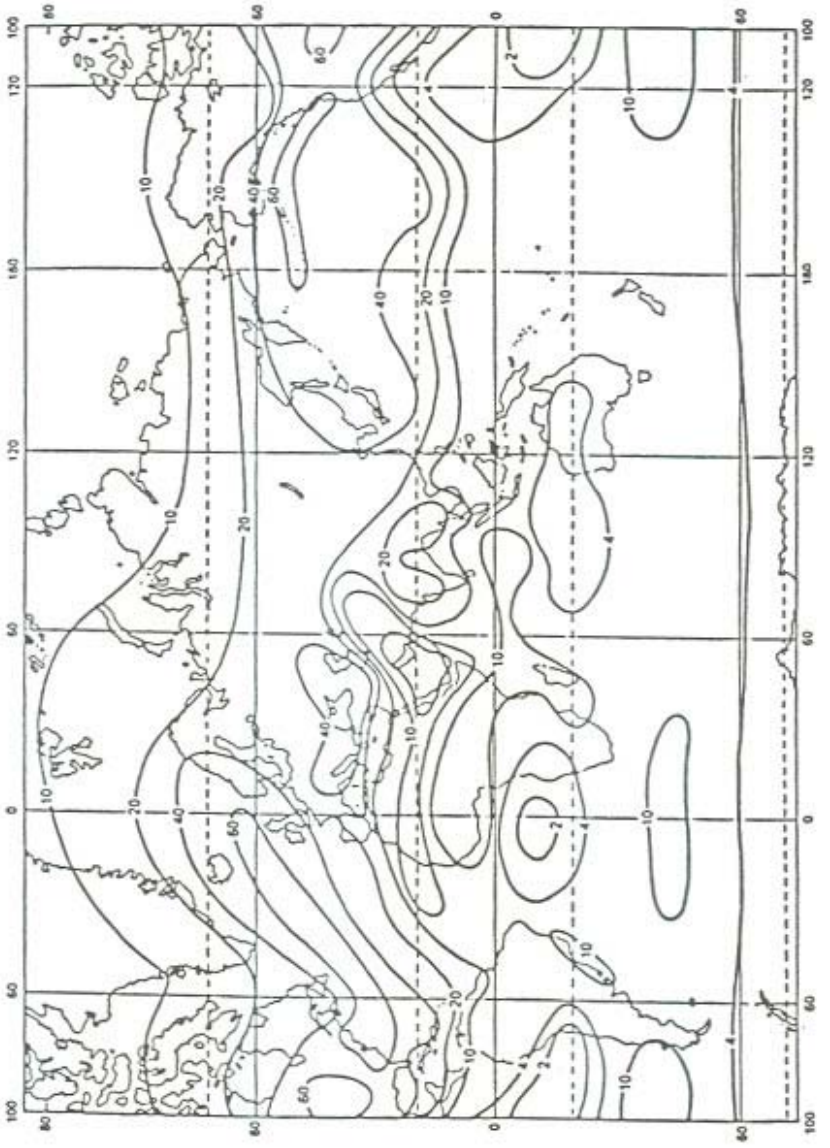

Figure 4.17 The distribution of ^{90}Sr at the Earth's surface 1963–1964.

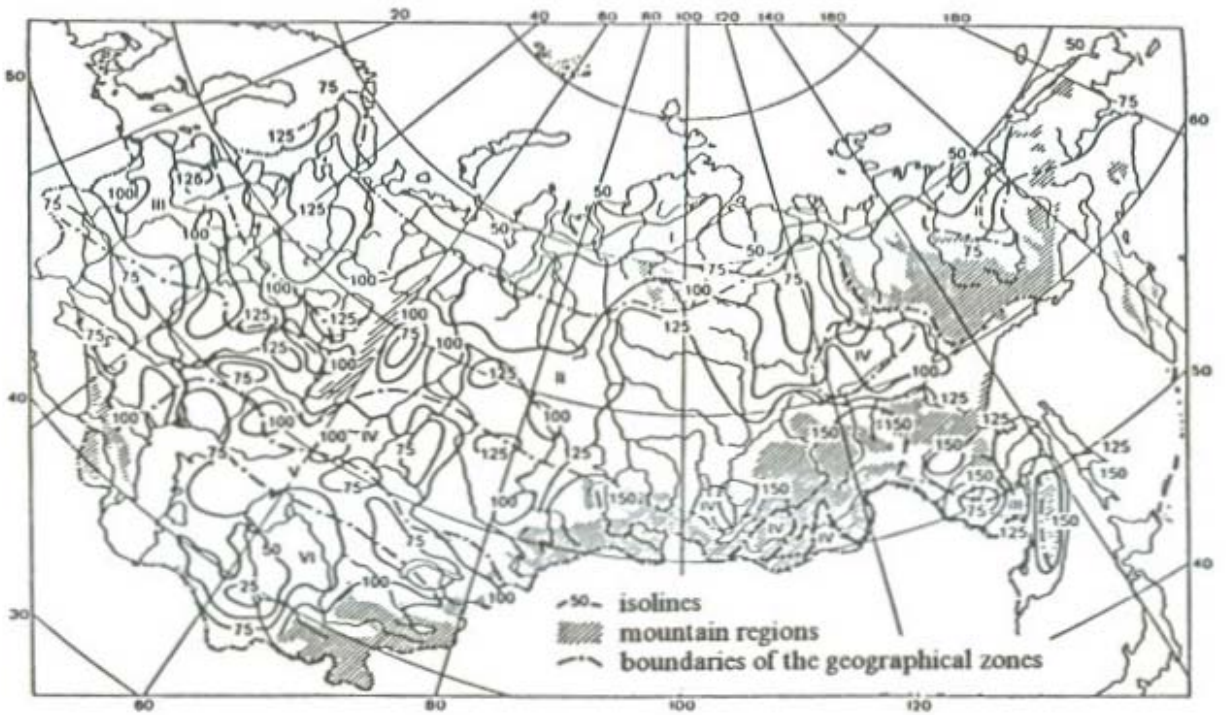

Figure 4.18 The ^{137}Cs contamination density in the former USSR (mCi km^{-2}) revealed by surveys conducted between 1968 and 1974.

altitude H there is a point source of a dispersed aerosol with distribution $N(W)$, for which the observed fallout pattern can be calculated (Petrov and Pressman, 1962; Izrael *et al.*, 1970a). The expression for the fallout pattern resulting from this distribution with an average wind velocity V is

$$p(x,y) = \frac{QHVN\left(\frac{HV}{x}\right)}{\sqrt{2\pi}\sigma_y(x)x^2} e^{-\frac{y^2}{2\sigma_y^2(x)}} \tag{4.9}$$

where Q is the total source strength (Bq), $\sigma_y(x)$ is the dispersion of the distribution $p(x,y)$ in the y direction (km) and $N(HV/x)$ is the volume density of the particles according to the particle settling velocity, $W = HV/x$.

The total radioactivity (in Bq) at $t = h + 1$ hours is related to the explosive power $\bar{P}$ (in kt) by $A_{\Sigma}(h+1) = 4.5 \times 10^8 \bar{P}$ and the dose rate can be related to the fallout pattern by

$$P(x,y) \cong k_1 p(x,y) \tag{4.10}$$

where $k_1 \approx \frac{10^{-5}\ R\ h^{-1}}{\text{Bq}\ km^{-2}}$, $h = 1$ m (h is height of the measurement of the dose rate).

For atmospheric explosions $Q = A_{\Sigma}$; for underground explosions $Q = A_{\Sigma} \times I(\bar{h})$, where is $I(\bar{h})$ is the fraction of the total radioactivity released into the atmosphere.

The term $\sigma_y(x)$ may be calculated using equation (4.11)

$$\sigma_y(x) = \frac{\int_{-\infty}^{\infty} p\ (x,y)\mathrm{d}y}{\sqrt{2\pi}\ p\ (x,\ 0)} \tag{4.11}$$

A function of distance from ground zero $\sigma_y(x)$ is described by

$$\sigma_y(x) = (\sigma_0^2 + 0.01x^2)^{1/2} \tag{4.12}$$

where σ_0^2 is related to the horizontal dimension of the main cloud and defines the transverse distribution near ground zero. It is possible to write for the volume density

$$N\left(\frac{HV}{x}\right) = \psi(w) = \frac{0.1\sqrt{2\pi}\ p_t(x,0)(HV)^2}{A \times I(h)} \tag{4.13}$$

Experimental data for explosions '1003', 'Sedan', 'Danny Boy', and 'Neptune' are used to determine the function $\psi(w)$ (see Figure 4.19). In this case $N(w) \approx$

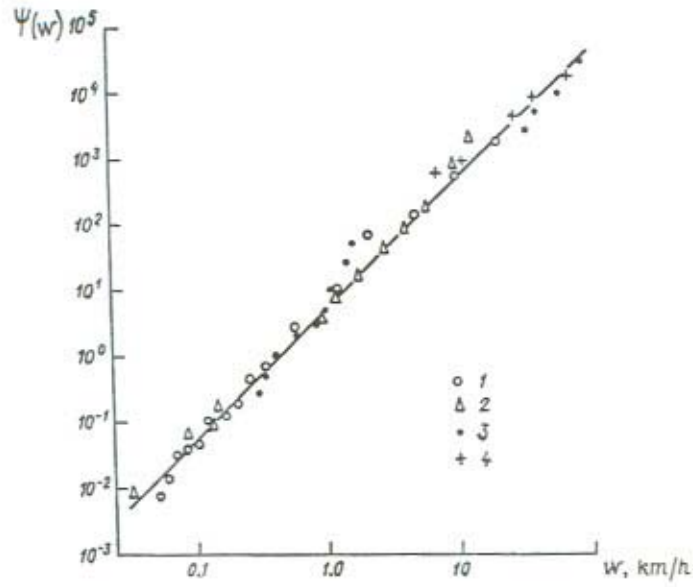

Figure 4.19 The dependence of volume density, $\psi(w)$, on w (particle settling velocity) for fallout patterns from explosions. (1) '1003', (2) 'Danny Boy', (3) 'Sedan', (4) 'Neptune'.

$1/w$ and the intensity for a radionuclide can be estimated by the appropriate function $\psi_i(w)$ using equation (4.9), in this case $Q_i = A_i \times I(\bar{h})$.

A calculation for the fallout patterns resulting from the detonation of a row charge of nuclear explosives may be made by means of equation (4.14) in which N explosives are placed in a line of length L. For the wind direction normal to the row, the doses D_N in the separate fallout tracks are given by

$$D_N(x,y) = ND_1(x,0)\sqrt{\frac{\pi}{2}}\frac{\sigma_y}{L}\left[\phi\left(\frac{L-y}{\sigma_y}\right)+\phi\left(\frac{y}{\sigma_y}\right)\right] \tag{4.14}$$

where $\phi(z) = \sqrt{2/\pi}\int_0^z e^{-t^2/2}dt$ is the probability integral.

If for D_1, the dose from a single explosion

$$\sigma_y^2 = (0.1x)^2; \text{ then } D_N(x,L/2) \approx ND_1(x,0) \tag{4.15}$$

with a maximum error of 17% when $L/2\sigma_y < 1$.

Figure 4.20 shows the long-distance radioactive fallout rate for test explosion '1003' using a deposition velocity of $\beta = 3.6 \times 10^{-2}$ km hr^{-1}.

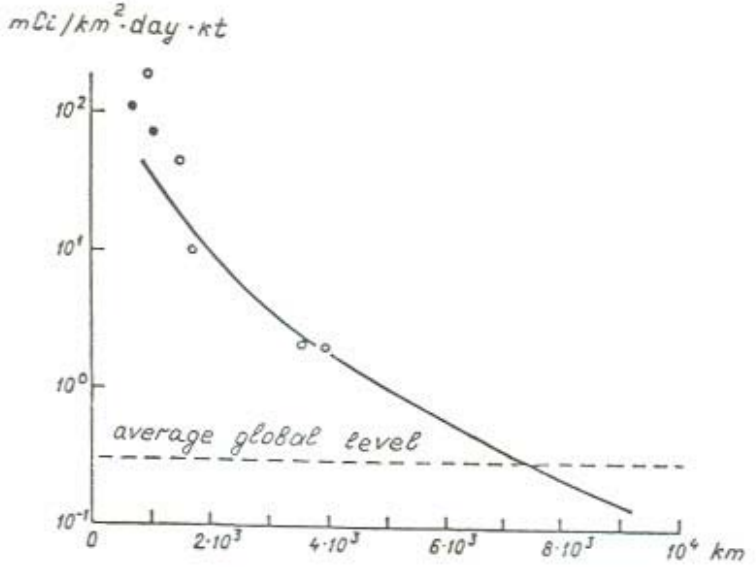

Figure 4.20 The relationship between the radioactive fallout rate and distance for an explosion yield of 1.1 kt.

4.3 LOCAL AND TROPOSPHERIC FALLOUT PATTERNS IN DIFFERENT COUNTRIES

4.3.1 French tests

The French nuclear tests in the atmosphere were carried out at Hamoudia near Reggane in the Algerian Sahara in 1960 and 1961 and on the uninhabited atolls of Mururoa and Fangataufa in French Polynesia from 1966 to 1974 (Doury and Musa, 1996). Fifty tests were carried out, four on barges (in 1966 and 1967), forty-one under other conditions (balloon, tower, aircraft) and five tests of very low energy, so-called 'for security'. The total energy of all tests is equivalent to 10 million tons (10 Mt) of TNT.

The report of Doury and Musa (1996) at the SCOPE-RADTEST Workshop in Beijing, 19–21 October 1996, included surface plots of four proximal (immediate) fallout patterns resulting from the atmospheric nuclear explosions that took place on the atolls of Mururoa and Fangataufa. The characteristics of the explosions are listed in Table 4.6.

The explosions differed from each other both in their power (from 34 to 955 kt), and the heights at which the nuclear devices were situated at the moment of the explosion (from 3 to 480 m). This illustrates the different relationships

Table 4.6 Characteristics of four atmospheric nuclear explosions conducted by France in the Southern Hemisphere.

Date	24.09.66	05.06.71	12.06.71	14.08.71
Name	Rigel	Dione	Encelade	Rhea
Type of explosion	Barge	Under an air balloon	Under an air balloon	Under an air balloon
Place	Fangataufa	Mururoa	Mururoa	Mururoa
Total power, kt	125	34	440	955
Height of the nuclear device at the moment of explosion, m	3	275	450	480
Height of tropopause, km	12.7	12.9	17.5	–
Height of cloud base, km	7.0	12.0	13.5	15.5
Height of cloud top, km	13	14	17	20

between the amount of the material deposited and the parameters of the explosions and meteorological situations. The pattern shown in Figure 4.21 is characterized by high-dose rate levels up to 100 rad (1 Gy) h^{-1} one hour after the explosion at a distance of up to 70 km, it corresponds to a powerful explosion (125 kt) and a low height of the nuclear device at the moment of explosion. These circumstances led to the generation of a large number of particles, resulting from the melting and evaporation of the device, the barge and seawater, which formed such an intensive pattern at distances exceeding 1000 km from the epicentre.

Figures 4.22–4.24 show configurations of the proximal (immediate) fallout patterns of three atmospheric explosions conducted with the help of air balloons. In spite of great differences in the power of the explosions (34, 440 and 955 kt) the observed dose rates differ only slightly from each other in their proximal (immediate) fallout patterns. They were found to be less than 1 rad (0.01 Gy) h^{-1} even 1 hour after the explosion.

The cumulative fission energy of the French tests can be estimated at 6500 kt, a little less than 3% of the world total. It represents, assuming that all the fission products are about evenly distributed world-wide, an average irradiation equivalent of 11 days of natural radioactivity. The low tropospheric values (in relation to the stratospheric values) are a beneficial result of the explosion technique called 'under balloon'.

4.3.2 UK tests

During the period from 1952 to 1991 the UK carried out 45 nuclear explosions, 21 (1952–1958) being atmospheric, and 24 (1962–1991) underground (*Bulletin of Atomic Scientists*, 1995). All the underground explosions were conducted

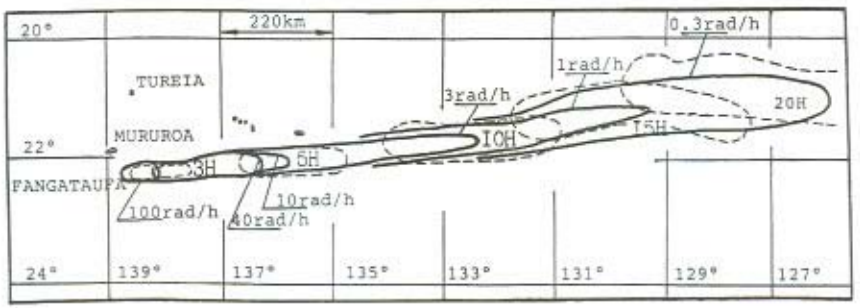

Figure 4.21 Proximal (immediate) fallout (isodose rates and isochrons) pattern of a 125 kt fission test explosion on a barge, Rigel, on 24 September 1966, at Fangataufa.

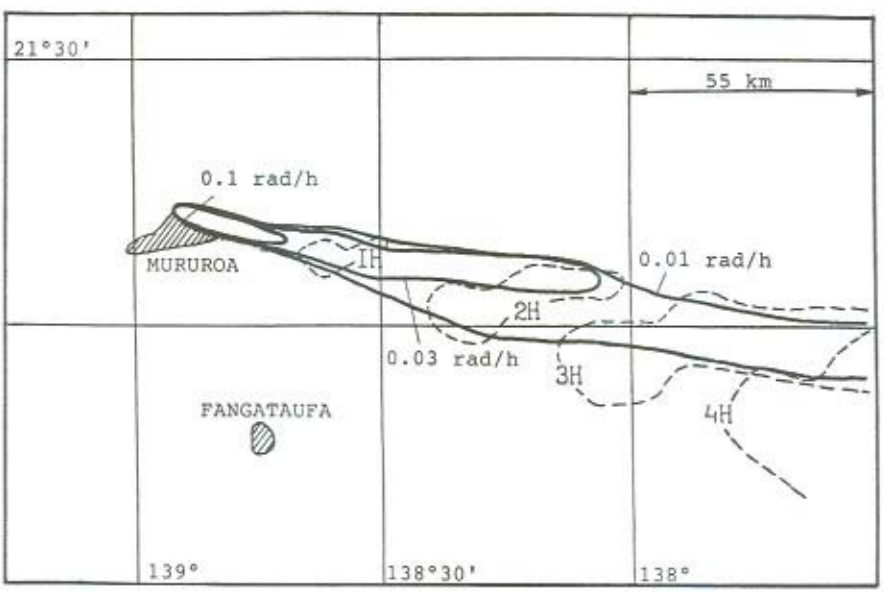

Figure 4.22 Proximal (immediate) fallout (isodose rates and isochrons) of a 34 kt fission test explosion beneath an air balloon (275 m), Dione, on 5 June 1971, at Mururoa.

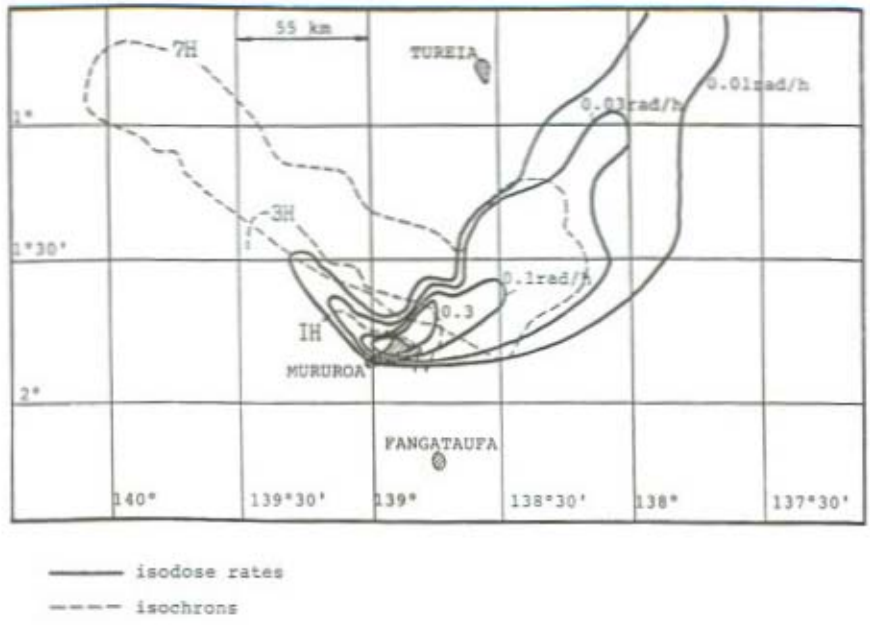

Figure 4.23 Proximal (immediate) fallout (isodose and isochrons) of a 440 kt fission test explosion beneath an air balloon (450 m), Encelade, on 12 June 1971, at Mururoa.

jointly with the USA. They were described in official publications (US DOE, 1994), under the name 'Joint US–UK'. They were conducted at the Nevada Test Site, and their nuclear devices were located in shafts.

On 3 October 1952, surface nuclear explosion 'Hurricane' on the western shore of Trimouille island initiated the atmospheric testing of nuclear weapons by the UK. The power of this explosion was equal to 25 kt (Norris *et al.*, 1994). Following this, from a report (Haywood and Smith, 1990) presented to the SCOPE-RADTEST Panel in Vienna in January 1994, the UK conducted some tests in the Maralinga and Emu areas (southern Australia) in the period of 1953–1957. In order to assess the potential irradiation doses that the future residents of these areas could be exposed to, research activities were conducted in these areas in the late 1980s. To this effect, in addition to the obvious studies, aerial gamma-spectrometric surveys were performed. Some results of these surveys of proximal patterns of ^{241}Am are shown in Figure 4.25 (Maralinga). Figures 4.26 and 4.27 show the values for ^{137}Cs at Maralinga and Emu respectively. As follows from Figure 4.25 the ^{241}Am patterns (from nuclear explosions with plutonium devices) are much pronounced and can be singled out and have more or less one initial position. Figure 4.26 shows quite another picture. Here individual ^{137}Cs patterns relating to separate explosions do not

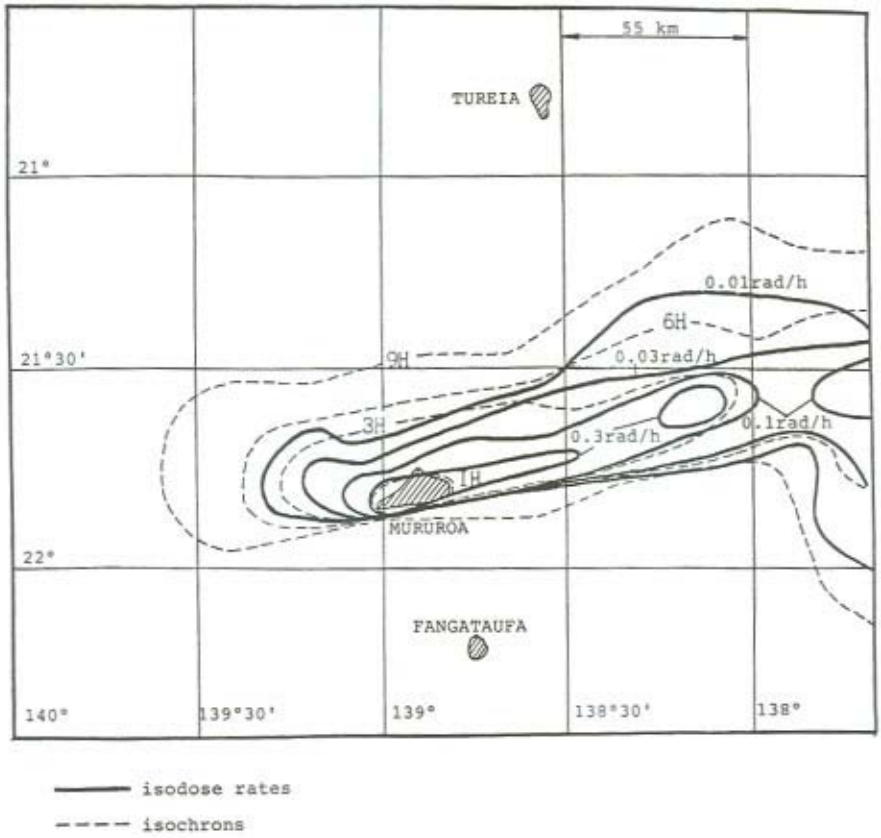

Figure 4.24 Proximal (immediate) fallout (isodose rates and isochrons) of a 955 kt fission test explosion beneath an air balloon (480 m), Rhea, on 14 August 1971, at Mururoa.

stand out against the general pattern of contamination. In contrast, we see two distinctly pronounced and separated ^{137}Cs patterns in the Emu area (Figure 4.27). This must be attributed to the fact that only two explosions (Totem-1, 14 October 1953 and Totem-2, 26 October 1953) were conducted in this area.

4.3.3 USA tests

For the period of nuclear weapons testing from 1945 to 1992 the USA carried out 210 atmospheric and nine crater nuclear explosions (US DOE, 1994). Among these explosions, 129 could potentially have led to surface patterns: 9 crater, 36 barge, 28 surface and 56 tower explosions.

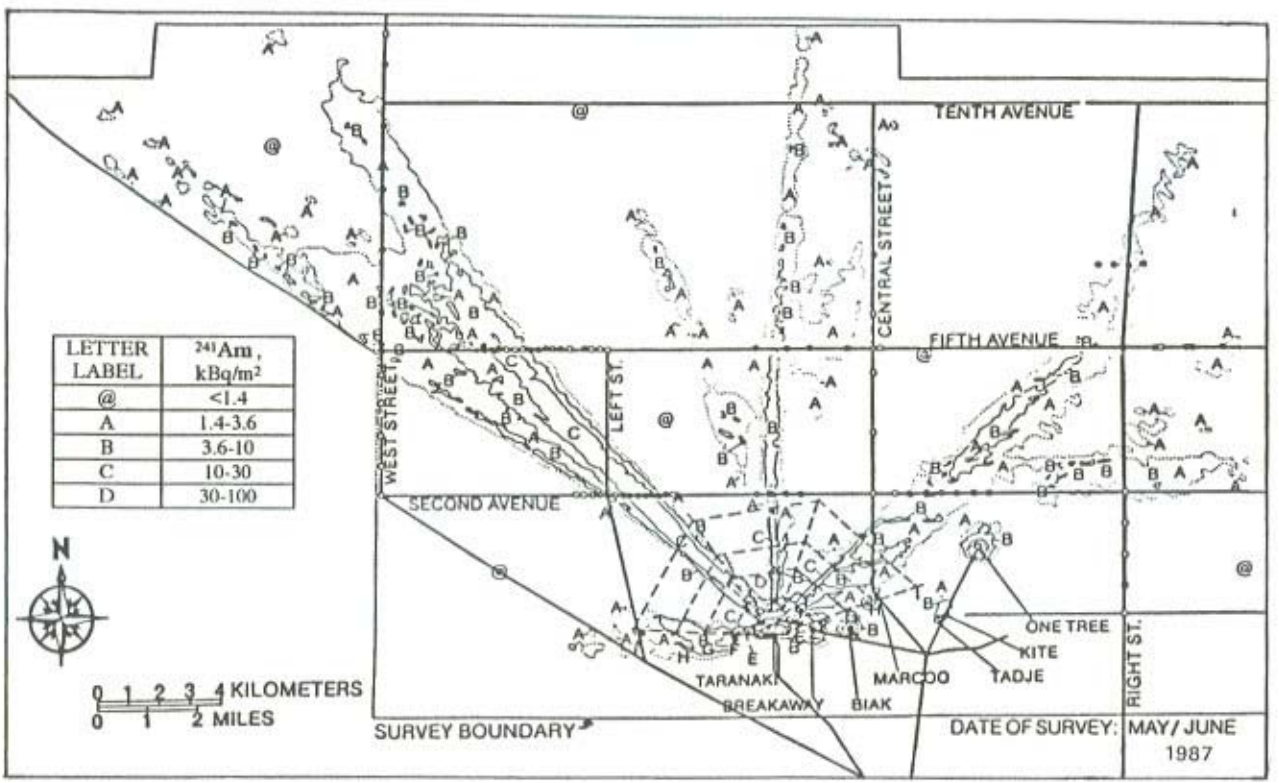

Figure 4.25 Contamination patterns for ^{241}Am in the Maralinga area.

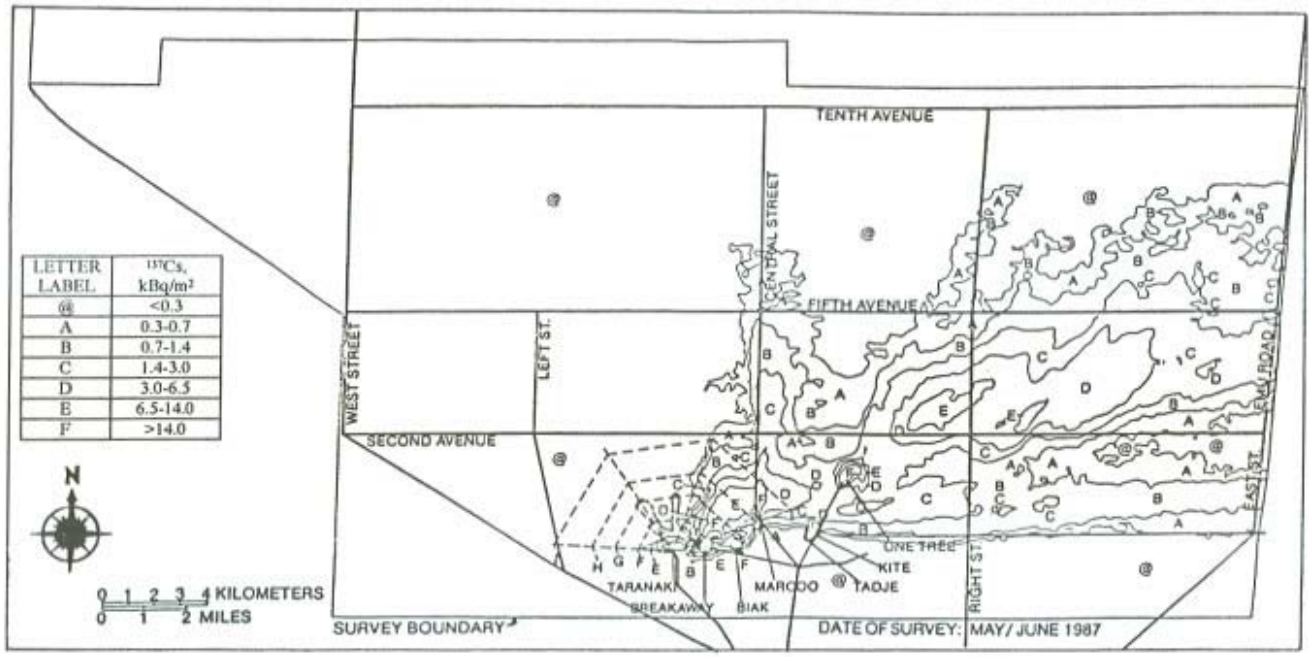

Figure 4.26 Contamination patterns for ^{137}Cs in the Maralinga area.

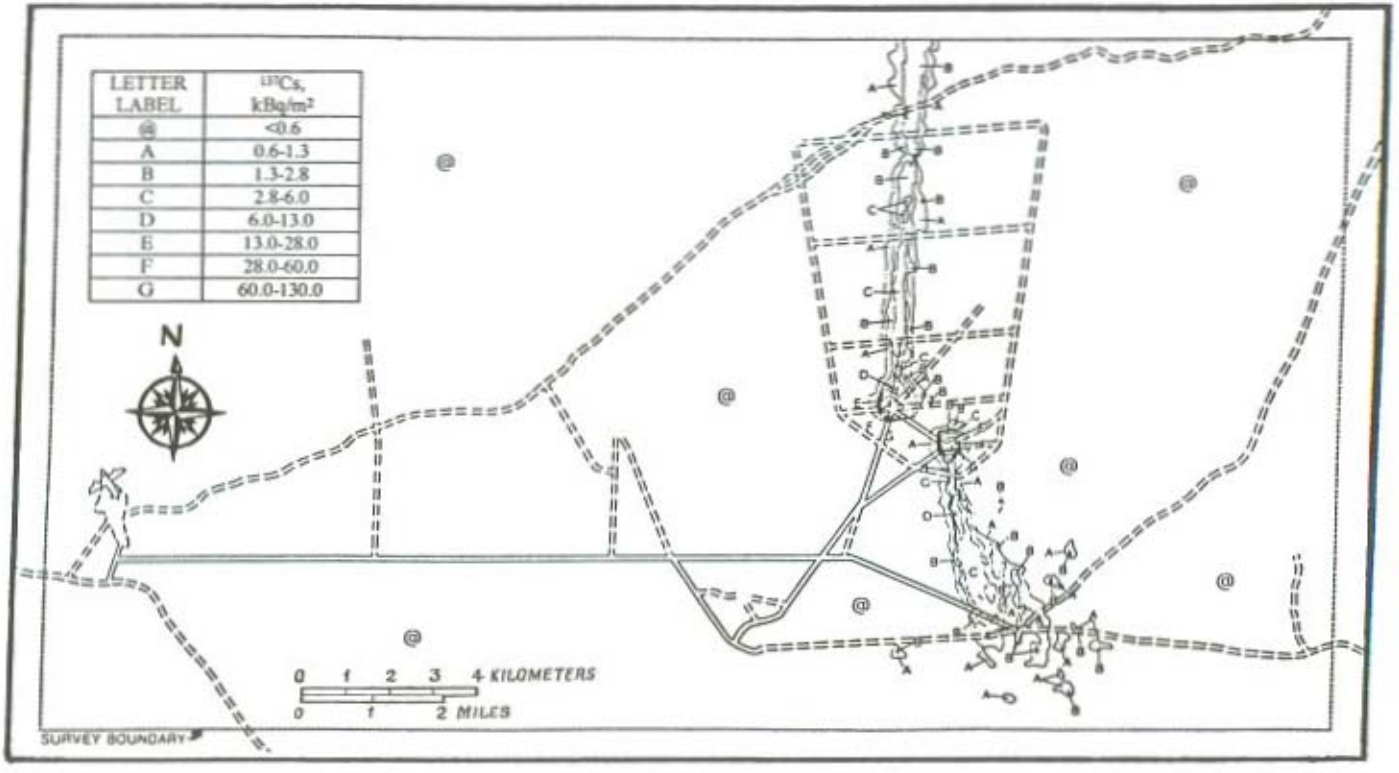

Figure 4.27 Contamination patterns for ^{137}Cs in the Emu area.

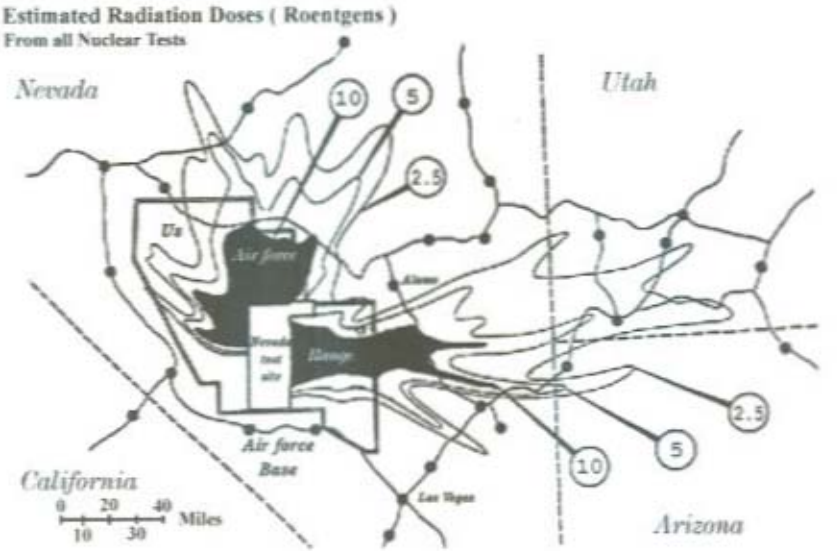

Figure 4.28 Contamination pattern from nuclear tests carried out at the Nevada Test Site up to 1958 (Dunning, 1959). See glossary for conversion of roentgens to grays.

During the testing, the open press published data concerning mainly the radioactive patterns that originated from the crater and surface explosions known as 'Plowshare'; namely 'Danny Boy' (5 March 1962), 'Sulky' (18 December 1964), 'Sedan' (6 July 1967), 'Cabriolet' (26 January 1968), 'Buggy A-E' (3 December 1968), 'Schooner' (8 December 1968). Some information on these explosions is shown in Table 4.3, and Figures 4.13 and 4.19.

Some literature data on the ground radioactivity patterns from single or multiple nuclear explosions are available. In 1959 a work entitled *Fallout from Nuclear Weapons Tests* was published in the USA (Dunning, 1959), in which a generalized map is presented on irradiation doses assessed over areas adjoining the Nevada Test Site for the whole test period before the 1958 moratorium. The map is reproduced as Figure 4.28: the total potential external exposure dose, in roentgens to humans outside the Nevada Test Site, should they have been at one of the points on a permanent basis, are given. At the same time one can assess from the same figure the integrated contamination pattern from the nuclear explosions conducted at Nevada Test Site before 1959: doses of up to 10 roentgens (86.9 mGy) are entirely located in the State of Nevada. Values of 5 (43.5 mGy) and 2.5 roentgens (21.7 mGy) are spread in patches over the States of Utah and Arizona. The densely populated State of California is practically not contaminated.

In the work *Radiological Conditions at the Bikini Atoll, Republic of the Marshall Islands: The Prospects for Resettlement* (IAEA, Vienna, 1996), the ^{137}Cs pattern contamination is provided of the 1993 mapping of soil contamination levels for Bikini Island at Bikini Atoll (Figure 4.29, dose rate, mGy y^{-1}). The survey was conducted in the framework of the Republic of the Marshall Islands Radiological Study (NWRS) using solid-state type detectors installed at a height of 1 m above the soil surface. The isolines of the soil ^{137}Cs contamination density (in a 10 cm layer) at Bikini Island (Bq g^{-1} of dry soil) are shown. These results were obtained by Lawrence Livermore National Laboratory in 1981using aerial gamma-spectrum measurements. The table in Figure 4.29 makes it possible to compare external exposure dose rates and soil contamination densities due to ^{137}Cs. The area of Bikini Island is less than 4.5 km^{-2}, the maximum density values of the soil contamination by ^{137}Cs in the 10-cm soil layer are around 12 Ci (444 GBq) km^{-2}. In addition to ^{137}Cs, the radionuclides ^{90}Sr, $^{239+240}Pu$ and ^{241}Am are fixed in the soil.

4.3.4 The former USSR tests

The main programme of nuclear weapon testing in the former USSR was carried out at the Semipalatinsk Test Site (STS), where on 29 August 1949 the first national nuclear explosion was conducted; and at the Northern Test Site Novaya Zemlya (NTSNZ), where the last explosion was carried out on 24 October 1990. The total number of nuclear tests conducted within the former USSR Test Sites is 586. In addition, according to the programme of peaceful use of nuclear explosions, 129 nuclear tests were carried out within the former USSR but outside the Test Sites, including 91 tests in the territory of the Russian Federation, two in Ukraine, 33 in Kazakhstan, two in Uzbekistan and one in Turkmenistan (Mikhailov *et al.*, 1996).

For the period of 1949 to 1962 at the Semipalatinsk Test Site, 25 ground nuclear explosions (Mikhailov *et al.*, 1996), i.e. those explosions where the expanding fireball touches the ground surface, were carried out. As a result great amounts of soil were swept into the explosion cloud.

Under these circumstances, particles may be activated and contribute to the radioactive fallout pattern in the direction of the prevailing winds. This pattern has been registered by radmeter equipment at a distance of hundreds of kilometres from the centre (epicentre) of the explosion considered, during the first days, weeks and even months after the explosion. A special survey method was established, which took the height of the flight and the terrain relief into consideration.

In this context it is essential to analyse the generalized map of the proximal fallout patterns (up to hundreds of kilometres) attributable to the STS nuclear tests (Figure 4.30). This generalized map was published for the first time by Logachov (1996). From this map it can be concluded that among the nuclear

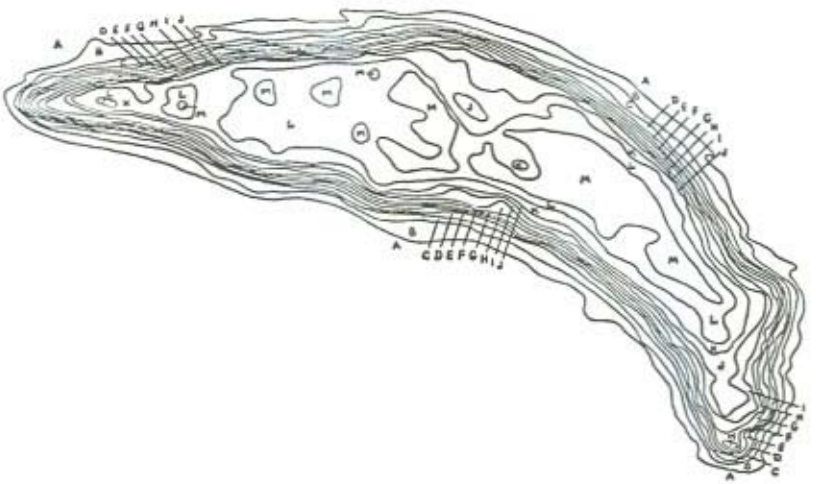

CONTOUR AREA	^{137}Cs Gamma Exposure Rate (mGy/a)	Average ^{137}Cs Activity in Top 10 cm of Soil (Bq/g)
A	< 0.009	< 0.007
B	0.009 - 0.026	0.007 - 0.022
C	0.026 - 0.055	0.022 - 0.048
D	0.055- 0.102	0.048 - 0.089
E	0.102 - 0.168	0.089 - 0.148
F	0.168 - 0.292	0.148 - 0.259
G	0.292 - 0.438	0.259 - 0.370
H	0.438 - 0.657	0.370 - 0.629
I	0.657 - 1.02	0.629 - 0.925
J	1.02 - 1.46	0.925 - 1.30
K	1.46 - 2.19	1.30 - 1.85
L	2.19 - 2.92	1.85 - 2.59
M	2.92 - 4.38	2.59 - 3.70

Figure 4.29 The ^{137}Cs gamma-radiation dose rate and average ^{137}Cs activity in the top 10 cm of soil on Bikini Island at Bikini Atoll.

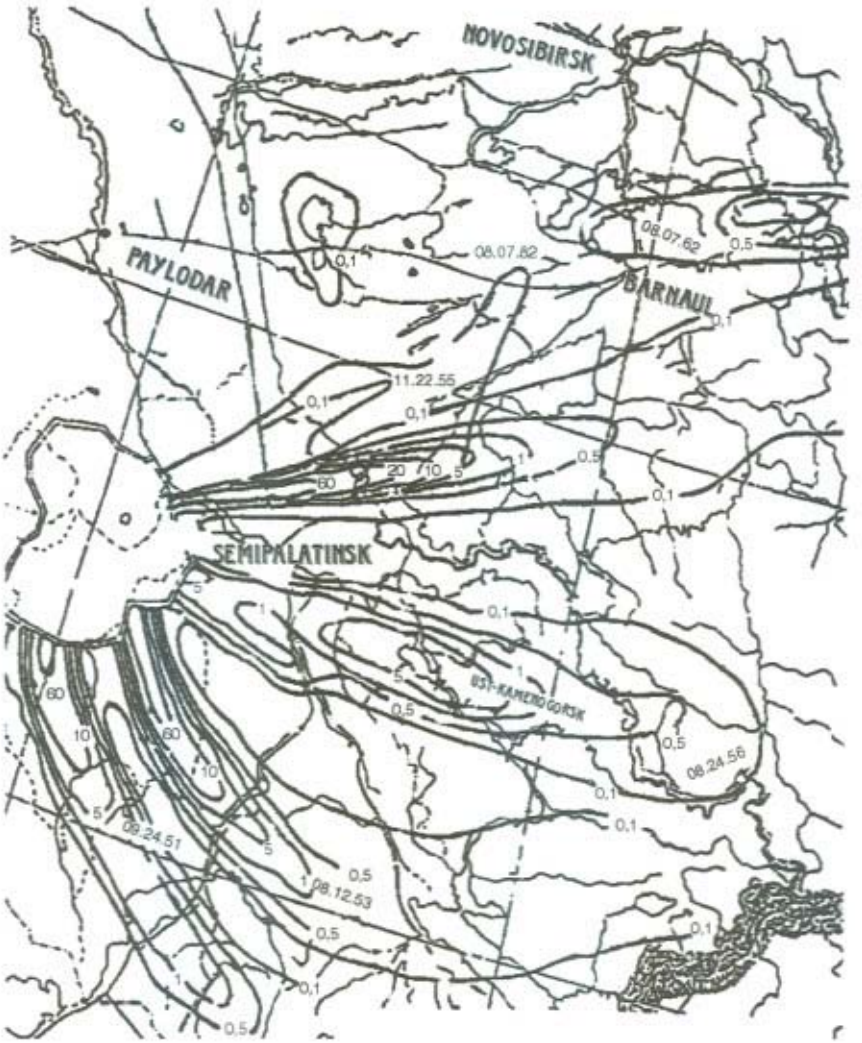

Figure 4.30 Map of fallout patterns from atmospheric and ground surface tests at the Semipalatinsk Test Site. Isodose lines give estimated cumulative unshielded doses on the ground (isodose lines are in roentgens; 24.09.51, etc., is the date of the relevant explosion).

test explosions the following have to be considered as capable of damaging the population of the nearby regions (mainly Semipalatinsk, eastern Kazakhstan and the Altai region of Russia): 29 August 1949 (22 kt, explosion on a tower, 30 m), 24 September 1951 (38 kt, explosion on a tower, 30 m), 12 August 1953 (400 kt, explosion on a tower, 30 m, the first thermonuclear explosion in the former USSR), 22 November 1955 (1600 kt, airdrop, height of explosion, 1550 m), 24 August 1956 (27 kt, explosion on a tower, 100 m), 7 August 1962 (9.9 kt, surface explosion) and 15 January 1965 (140 kt, underground crater explosion). The isolines shown on the map present the total external dose after the complete decay of all the radionuclides.

An airborne gamma-spectrum survey in 1991 was carried out by the Scientific Production Enterprise 'Aerogeologiya', mainly within the STS. It displayed the existence of patterns which can still be observed. They are characterized by levels exceeding 300–500 mCi (11.1–18.5 GBq) km^{-2} attributable to ^{137}Cs, originating from the following nuclear explosions: 29 August 1949, up to 12–18 km in a direct line from the epicentre (probable); 24 September 1951, up to 55–65 km; 12 August 1953, up to 80–95 km; and 15 January 1965 ('Chagan'), up to 13–18 km (see Figure 4.9). As can be seen from Figure 4.9, beyond these distances the pattern of contamination cannot be outlined by a single continuous isoline, and they become indistinguishable from the regional and then the global background fallout levels.

Some information on these and other explosions is provided in Table 4.3 and in Figures 4.8, 4.9, 4.11, 4.12, 4.14, 4.15 and 4.16.

4.3.4.1 The First Nuclear Explosion in the former USSR in 1949

The first test of a nuclear weapon was performed in the former USSR on 29 August 1949. The nuclear device was mounted on a tower at a height of 30 m. The energy release was about 22 kt. The upper nuclear cloud edge reached a height of 7.5–9.0 km. The weather at the time of the nuclear test was very unstable: intermittent rain accompanied by strong gusts. The medium wind speed in the transport layer was 40–60 km h^{-1}, with gusts up to 75 km h^{-1}.

A week later, on 5 September an aerial radiation survey was carried out beginning with the settlement of Dolon located near the STS boundary towards the town of Bijsk. In the period from 7 to 13 September a ground-based survey was performed in human settlements and along the route of the automobile radiation patrol. The gamma-ray intensity was measured using the same instrument. Gamma-radiation, dose-rate airborne measurement data were scaled to a height of 1 m above the ground surface with the help of height coefficients characteristic of a non-fractionated mixture of ^{239}Pu fission products of an age of one week. All measurements were carried out at time $D + 7$ according to the Way–Wigner law, with a decay exponent of $n = 1.2$. These archive data available at STS at the beginning of 1993 are presented in Figure

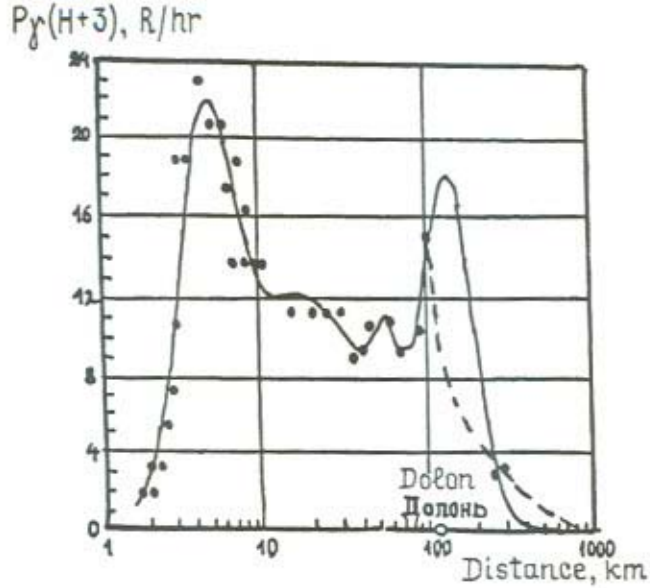

Figure 4.31 Airborne gamma dose rates (filled circles) one week after 29 August 1949 explosion at STS. The continuous line shows experimental data and the possible shape of the curve is shown as a dashed line. The figure is taken from Andrushin *et al.* (1994).

4.31 as filled circles. Approximation of the experimental data carried out at STS is shown as a continuous line (Andrushin *et al.*, 1994), and a dashed line shows the possible shape of this curve.

A reconstructed area of the radioactive fallout pattern, as isolines of gamma-ray doses at complete decay of radioactive fallout, is shown in Figure 4.32. Taking into account the possible errors that could occur when measuring gamma-ray dose rates, calculating exposure doses and interpolating to determine the position of dose isolines, it can be asserted that the maximum error for the terrain gamma-ray dose does not exceed +100%.

4.3.4.2 Formation of an Artificial Reservoir (crater explosion '1004')

On 15 January 1965 the first underground nuclear explosion to create a crater was carried out at the confluence of two rivers—Chagan and Achan-Su. A nuclear device with a power of 140 kt was ignited at a depth of 175 m in slightly watered sandstone with an admixture of lignite–clayey schist. The power originated from the fission reaction is 7 kt of the total value (Mikhailov *et al.*, 1996). As a result of the explosion, a crater was formed with a diameter 400–430 m at the original ground surface, and a depth of about 100 m. Its volume was 6×10^6 m^3.

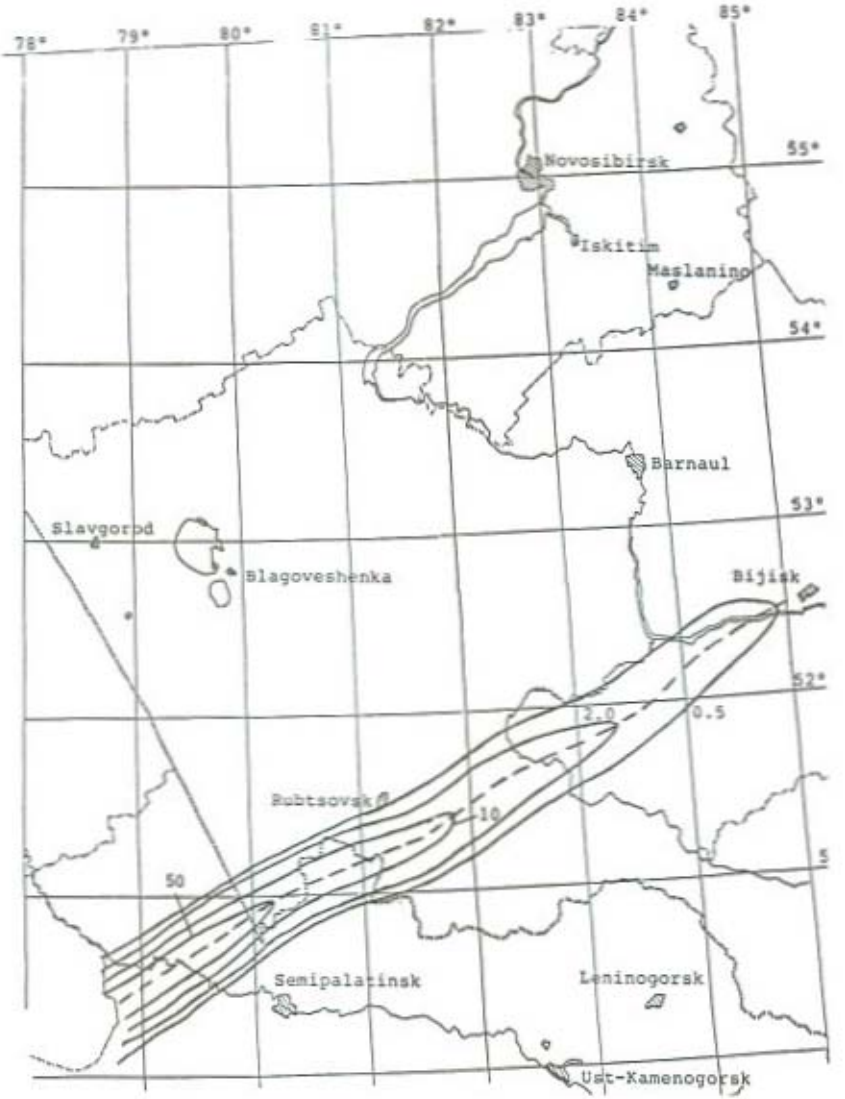

Figure 4.32 Integrated gamma-radiation dose distribution until the complete decay of radioactive fallout (roentgens) for the surface explosion of 29 August 1949.

A characteristic feature of this explosion was the generation of a powerful base surge (by the middle of the second minute), with a diameter 5000 m and a height reaching 2.5 km. It spread to the north, and a formation in the shape of a pillar with a height of up to 2.5 km moved in a northeastern direction. The stabilization height of the radioactive cloud of the explosion was 4.5–4.8 km. The distribution of the radioactivity with depth in the zone of the base surge is shown in the Figure 4.11.

Observation of the radioactive contamination in the proximal zone during the period of immediate radioactive fallout, and also after this period, was carried out by means of ground-based and airborne radiation surveys. Of the total amount of radioactive products generated by the explosion about 20% was deposited within the proximal zone during the immediate phase.

Figure 4.33 shows a map of the radioactive fallout pattern, presented as dose-rate isolines at the ground surface, in mR h^{-1}, 24 h after the explosion. This map was compiled on the basis of an air gamma survey of the territory during the first two days after the explosion.

At present, the mean radiation level is about 0.2 mR (1.7 μGy) h^{-1} in the epicentre zone of the explosion, reaching 4–8 mR (35–70 μGy) h^{-1} at certain observation points. The main gamma emitters are ^{137}Cs and the long-lived radionuclides of induced activity, ^{60}Co and ^{152,154}Eu.

4.3.5 Chinese tests

China started atmospheric nuclear explosion testing in 1964, and a total of 22 tests were conducted (Zhu Changshou *et al.*, 1996), as reported during the SCOPE-RADTEST Workshop in Beijing 13–21 October 1996. In their report to the same Workshop, Zheng Yi *et al.* (1996) referred to the fact that 'the data on yield and type of nuclear burst of these are quoted from the paper by De Geer'. At the Workshop (Beijing, 19–21 October 1996), De Geer presented a report 'Chinese Atmospheric Nuclear explosions from a Swedish Horizon' in which he included a summary of Swedish observations of Chinese nuclear test explosions in the atmosphere during 1964–1980, and Chinese experts presented a number of reports on the problem of radioactive deposition monitoring across the territory of China.

Since the end of 1950 a survey of radioactive contamination in the environment has been conducted in China. A system of investigation and a monitoring network for environmental radioactivity was organized by the Ministry of Health in the early 1960s, and operated by the sanitary–epidemiological stations and medical institutes in every province, autonomous region and municipality throughout China, forming a nation-wide environmental radioactivity monitoring network of 45 stations. The Laboratory of Industrial Hygiene of the Ministry of Health acts as the technical guidance centre.

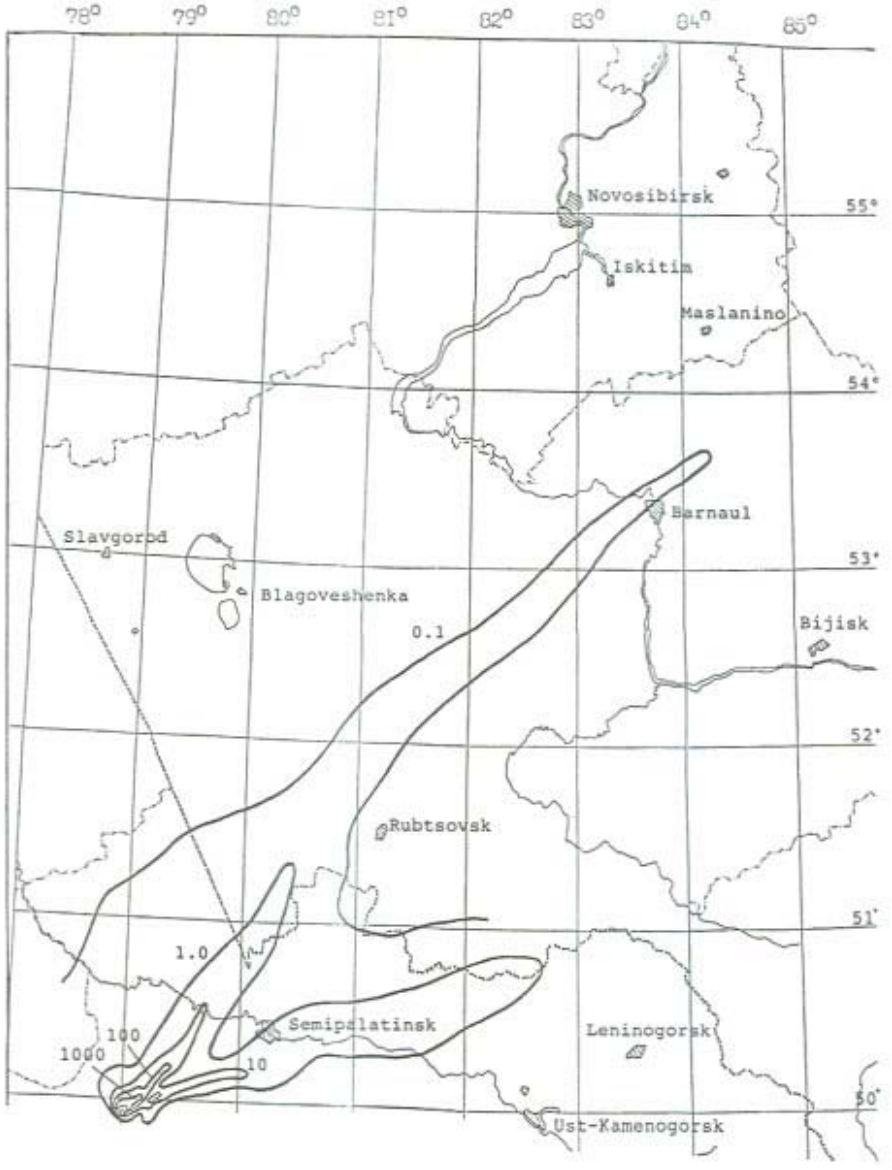

Figure 4.33 A map of dose rate distribution following the crater explosion 'Chagan', 15 January 1965, mR h^{-1} at 'H + 24'.

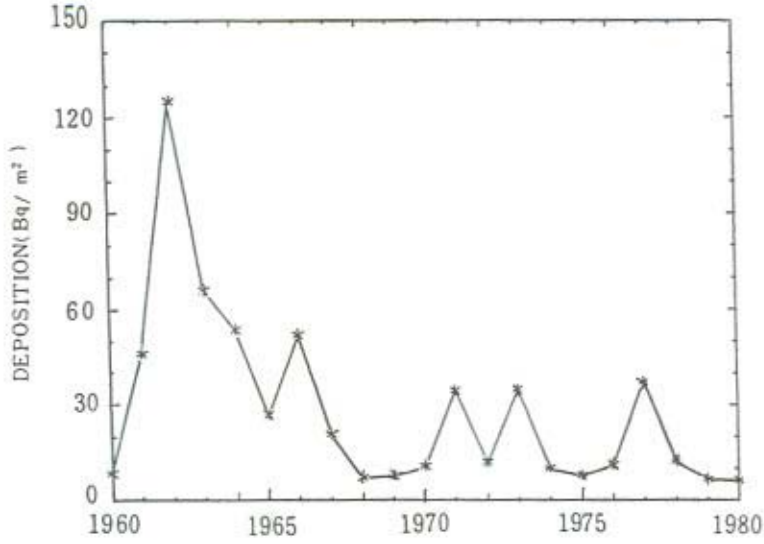

Figure 4.34 Variation of the annual average daily deposition of gross beta activity in China.

The gross beta activity in atmospheric fallout is a simple and sensitive indicator for monitoring the short-term pattern of contamination from radioactive fallout. Monitoring results show that the peak value of the annual average daily deposition of gross beta activity occurred in 1962, which was the result of early fallout from large-scale nuclear weapon explosions in 1962 in central Asia. Smaller peaks occurred in 1966, 1971, 1973 and 1977, registering the radioactive contamination from atmospheric nuclear tests conducted in China (Figure 4.34) during those years.

Environmental contamination from ^{131}I following nuclear explosions was observed in some regions of China. The short half-life of ^{131}I means that it is not well mixed in the atmosphere before deposition or decay. Consequently, concentrations in air or deposition at particular sites vary with meteorological conditions and are not necessarily representative of a larger region nor of a latitudinal band. Environmental contamination of ^{131}I following nuclear explosions in some regions such as in Lanzhou, Xining and Shenyang, was significant. The levels of radioactivity attributable to ^{131}I in some regions in China are listed in Table 4.7. The variation in levels of radioactivity attributable to ^{131}I after the fifth nuclear test in Shenyang is shown in Figure 4.35. The peak value of radioactive contamination by ^{131}I was about 710 Bq m^{-2}. The increased level of radioactive contamination from this source continued for 10 days (Figure 4.35).

Table 4.7 Deposition of ^{131}I in some regions in China.

Test number	Region	Deposition (kBq m^{-2})
4	Xi'an	0.33
5	Shenyang	4.8
12	Lanzhou	5.1
15	Lanzhou	10
18	Hohhot	0.22
22	Xining	10

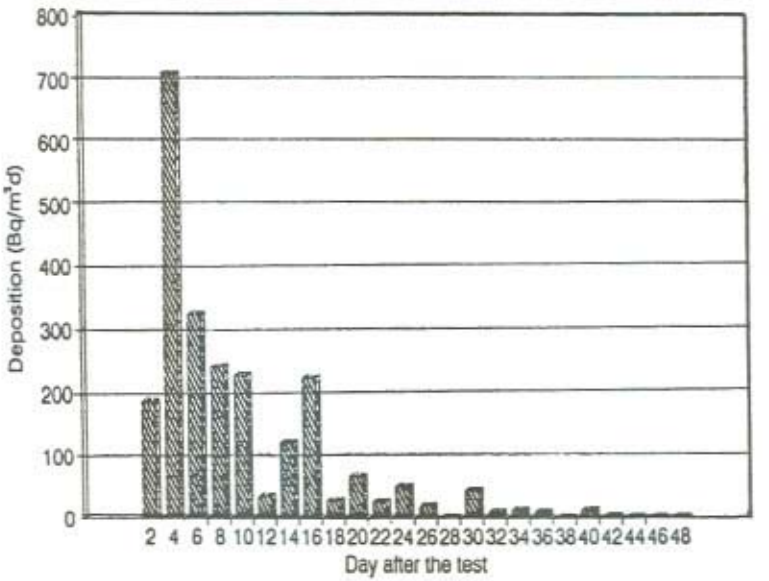

Figure 4.35 Levels of radioactivity as a result of the deposition of ^{131}I after the fifth nuclear test in Shenyang.

4.3.6 Indian tests

It is well-known that in 1974 India carried out an underground nuclear explosion, the only one in its programme at that time. The explosion took place in the Rajasthan Desert (Pokran) on 18 May 1974. Its power was equal to 12 kt. Indian specialists aimed to make this explosion completely contained to prevent any release of radioactive products to the atmosphere. All the material on this problem for inclusion in SCOPE-RADTEST was presented by Dr Mishra, who

sent them to Essex on 6 March 1997. Nevertheless, in carrying out the contained explosion, the Indian specialists took complex measures to cope with possible situations arising from releases to the atmosphere. Some of the measures were taken before the explosion, other were taken afterwards.

As an important part of the public and environmental programme for the experiment, a network of meteorological stations located very near surface ground zero was set up several months before the experiment. The climatological data from three meteorological stations (about 100 km from the site in various directions) for three decades and hourly surface and upper atmospheric wind observations from April to June of 1972 and 1973 were examined for planning the experiment. Also 24-, 48- and 72-h forecasts were available to warn of unusual weather changes such as cloudiness, storms, dust storms, etc., if any. On the basis of these observations and site topological considerations, the following conditions of the experiment were arrived at:

1. wind direction from the SW to W, preferably WSW;
2. wind speed—minimum 15 km h^{-1}, maximum 20 km h^{-1};
3. atmospheric stability;
4. no temperature inversions.

These criteria ensured that in the unlikely event of release of radioactivity and formation of a radioactive cloud, the expected direction of cloud travel would have been towards an uninhabited region, i.e. in the ENE sector, until the predicted maximum radiation exposure resulting from the passage of the cloud and deposition of radioactivity on the ground surface reaches insignificant levels.

The wind direction at the time of the experiment was WSW at a mean speed of about 20 km h^{-1}. The experiment was planned to be executed at a time when this wind direction was very constant and corresponding meteorological conditions were favourable. Atmospheric parameter measurements made by a ground-level barograph within a few kilometres of surface ground zero gave no indication of any air blast due to the release of cavity gases.

In addition to two health physics laboratories, a large amount of field monitoring equipment was kept ready. Equipment for on-the-spot checking of fission product contamination of water and vegetation was also provided. Prior to the experiment, several deposition trays and thermoluminescent dosimeters were distributed on a radial grid at 11.25° angular spacing and varying distance intervals. Extensive radiation monitoring of the site and analysis of samples before and after the experiment showed that no radioactivity had been released to the atmosphere during the experiment.

Five underground nuclear explosions (Table 4.8) were carried out by India during the period 11–13 May 1998 at the Pokhran range in the Rajasthan Desert. Their parameters were published in *BARC News Letter*, 172, May 1998.

Table 4.8 The five underground nuclear tests carried out by India in May 1998.

Type	Time	Date	Estimated yield (kt)
Thermonuclear	15.45	11.5.98	45
Fission	15.45	11.5.98	15
Experimental	15.45	11.5.98	~ 0.2
Experimental	12.21	13.5.98	~ 0.5
Experimental	12.21	13.5.98	~ 0.3

4.4 RECONSTRUCTION OF FORMER FALLOUT PATTERNS USING MATHEMATICAL MODELS AND ARCHIVAL DATA

The reconstruction of radioactive patterns and of possible exposure doses of the population from nuclear explosion tests seems a priority task. The reconstruction of radioactivity contamination patterns means the restoration of their main characteristics based on available but incomplete data about the source, the weather conditions, the dose rate, and the distribution of radionuclide contamination. Usually reconstruction has involved the restoration of contamination by patterns formed by incidents that occurred many years previously. Interest in the problems of reconstruction has increased much since the Chernobyl accident.

Modelling of radioactive fallout from past nuclear explosions seems necessary in order to reconstruct (or to be more precise, to construct) the patterns of radioactive contamination, i.e. assess the configuration of the contamination pattern.

In order to perform the reconstruction, it is also necessary to restore the meteorological situation at the time the nuclear tests were conducted. As an aid to reconstruction, use is made of information about the radioactive contamination patterns resulting from previous explosions.

When solving the problem of the transport of contamination from different types of sources, use is made of either numerical methods, for solving a three-dimensional turbulent diffusion equation, or various versions of the Monte Carlo method.

This section deals with the spread of contaminants in the atmosphere based on the trajectory model for particle transport in an inhomogeneous wind field when random deviations from trajectories simulating particles diffusion in the turbulent atmosphere are superimposed on the ordered particle motion. Such approaches have been used in a number of studies, e.g. when implementing the programme on assessing models of long-range radionuclide transport and comparing calculation results with data on radioactive deposition from the Chernobyl accident (the ATMES Programme), established by the CEC in

1992. This calculation technique uses both a one-step for integrating a particle motion equation based on the interpolation formula for horizontal wind speed components and a procedure of plotting random deviations of particle coordinates at each step of the integration. Random deviations, different for different particles, lead to the scatter of their trajectories in space, and, finally, to the scattering of particles depositing on to the underlying surface. The simulation modelling of scattering contaminants consists in this case in the selection of a distribution parameter of random deviations for each step to obtain a correspondence to the real distribution characteristics of deposited radioactive particles in the cloud pattern.

It is found that horizontal scattering of contaminants is approximately described by a two-dimensional Gaussian distribution with a standard deviation

$$\sigma_x(t) \approx \sigma_y(t) \tag{4.16}$$

For the time interval of 1–2 days the standard deviation $\sigma_{x,y} = \alpha\, l(t)$ (Izrael *et al.*, 1970a) varies with the distance from ground zero $l(t)$ (scattering regime 1), whereas for long time intervals $\sigma = \sqrt{2Kt}$ (regime 2).

The increment of dispersion from one act of a random deviation of particle coordinates to another is, for the first regime

$$\Delta\sigma_{j-1}^2 = \alpha^2 l_j^2 - \alpha^2 l_{j-1}^2 = \alpha^2(2\, l_{j-1} + \Delta\, l_{j-1})\Delta\, l_{j-1} \tag{4.17}$$

where $\Delta\, l_j = l_j - l_{j-1}$ is the distance travelled by the particle along its trajectory between scattering acts. For the second regime

$$\Delta\sigma_{j-1}^2 = 2K\,(t_j - t_{j-1}) = 2K\,\Delta\, t_{j-1} \tag{4.18}$$

where Δt_{j-1} is the time interval between scattering acts.

The sum of random deviations specified in the simulation process as $\sum_{j=1}^{n} C_j\gamma_j$, where γ_j is the sequence of accidental (in quasi-stochastic calculations) numbers equiprobably located in the interval [–1/2, 1/2] with a dispersion $\sigma_\gamma^2 = \frac{1}{12}$ and $C_j\sqrt{\Delta\sigma^2/\sigma_\gamma^2}$, determines regimes 1 and 2, correspondingly.

Particles which appeared random (n) form a symmetrical distribution $\pm\frac{1}{2}\sum_{j=1}^{n} C_j$ relative to the zero deviation, with a distribution density maximum at this point (for $n \geq 2$). There are no particles outside the said interval. The interval becomes longer as n increases, and for a limited number of deviations from the centre the distribution asymptotically approaches normal. The best result can be obtained when using group values $\frac{1}{\sqrt{m}}\sum_{i=1}^{m}\gamma_{ji}$ rather than accidental values.

The time step between the acts of particle dispersion is assumed to be constant, Δt = 1 h. The points where the particle is subjected to dispersion according to the initiation process can be dozens of kilometres apart. Even the spatial distribution of these points for the totality of the particles under consideration, is obtained by random variation of the initial step within the limits from 0 to Δt up to the first act of dispersion for different particles. It also

provides filling of the whole time period $t > 0$ by acts of dispersion when the number of particles is great.

In the interval between scattering acts one calculates the horizontal particle displacement in the wind field and its settling out by gravity. The particle coordinate values obtained at the end of the interval are supplemented by the random (quasi-stochastic) deviations referred to above, and a new particle location becomes initialized for the next interval of the ordered particle motion, etc., until its deposition on to the underlying surface.

In addition to particle gravitational deposition one takes into account capture by the underlying surface in the surface air layer, by adding the capture rate to the deposition rate, which can have an important influence on the deposition of finely dispersed fractions.

Horizontal particle transport is calculated based on data from the objective analysis of the three-dimensional wind field, presented in the form of latitude and longitude wind speed components on a uniform $2.5° \times 2.5°$ grid for standard isobaric levels. The particle horizontal coordinates are calculated in units of a specified grid $\Delta G = 2.5°$. For this purpose, U and σ_x are multiplied by $180/\pi R \cdot \Delta G \cdot \cos\varphi$, and V and σ_y are multiplied by $180/\pi R \cdot \Delta G$, where R is the Earth's radius and φ is the geographical latitude.

The angular displacement speed specified at the four corners of the square grid under consideration are interpolated to an internal point in the cell (including the cell boundary) by the formulae

$$U = \mathrm{d}x/\mathrm{d}t = U_1 (1 - x)(1 - y) + U_2 x (1 - y) + U_3 xy + U_4 (1 - x) y$$

$$V = \mathrm{d}y/\mathrm{d}t = V_1 (1 - x)(1 - y) + V_2 x (1 - y) + V_3 xy + V_4 (1 - x) y \quad (4.19)$$

where $0 \le x \le 1$, $0 \le y \le 1$ are the local coordinates relative to the left lower cell angle (U_1 V_1), and the corners are numerated counter-clockwise.

To integrate the systems of equations (4.19) together with the equation for particle gravity settling

$$\mathrm{d}z/\mathrm{d}t = - W \quad (4.20)$$

one applies a one-step algorithm, where the solution is given in the form of the Taylor series segment (Demidovich *et al.*, 1967).

$$x_{i+1} = x_i + x'(t_i)\Delta t + \frac{1}{2!} x''(t_i)(\Delta t)^2 + \frac{1}{3!} x'''(t_i)(\Delta t)^3$$

$$y_{i+1} = y_i + y'(t_i)\Delta t + \frac{1}{2!} y''(t_i)(\Delta t)^2 + \frac{1}{3!} y'''(t_i)(\Delta t)^3$$

$$z_{i+1} = z_i - \mathrm{W}\cdot\Delta t \quad (4.21)$$

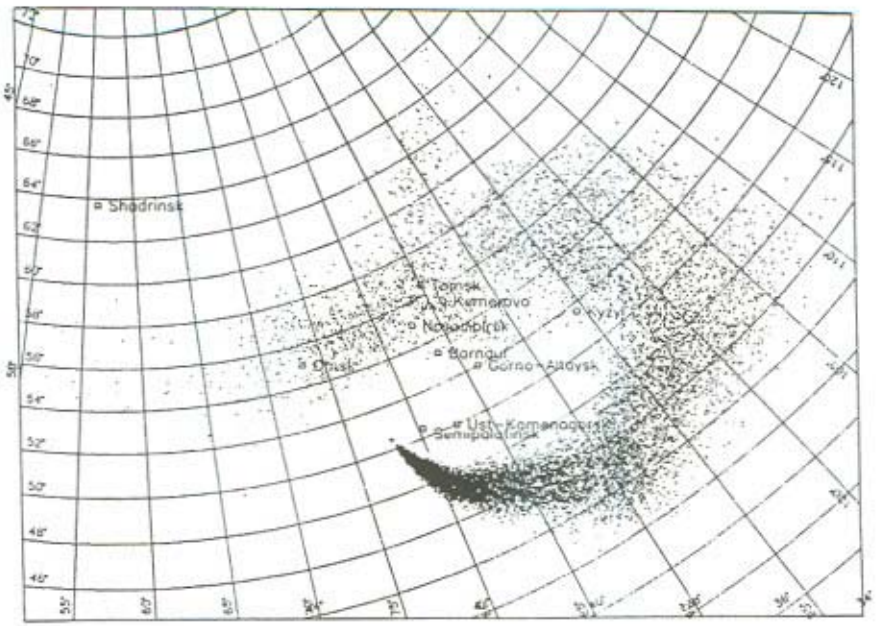

Figure 4.36 Map of calculated particle deposition from the nuclear explosion of 12 August 1953 at the Semipalatinsk Test Site.

where derivatives of the second and higher orders are found through a sequential differentiation system (equation 4.19).

Deposition of contaminants onto the underlying surface is calculated in two stages. In the first stage, one specifies in a source a fictitious particle distribution with gravity sedimentation rates. This provides their relative number in the deposition region under consideration. The coordinates of each particle deposited are calculated.

In Figure 4.36 a map is shown with particles deposited from the nuclear explosion of 12 August 1953 at the Semipalatinsk Test Site. The distribution density of the number of particles of all fractions with height is shown in the form of a truncated symmetric Gaussian distribution $9.6 \leq h \leq 15$ km with a maximum distribution density five times as much as that at the boundaries (h is the height of the middle of the cloud).

In the second stage of the calculation one determines the total particle activity for each fraction in accordance with the lognormal distribution of activity over the particle diameter. The deposited particle coordinates found at the first stage (discrete activity distribution) are considered as centres of supplementary continuous activity distribution of fictitious particles on to the underlying surface. This provides a calculation of depositional density and smoothes the statistical scatter of the design data.

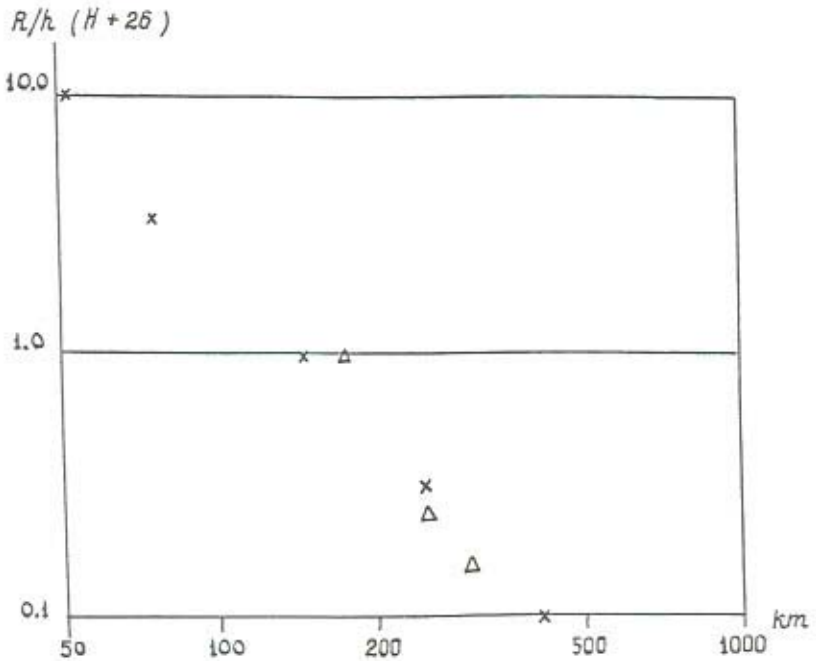

Figure 4.37 Dose rate values in the axis of the cloud pattern after the nuclear explosion of 12 August 1953, 26 hours after the explosion; Δ, measured values (Logachov, 1994); x, calculated values.

For example, one calculates the dose rate distribution in the cloud pattern from the surface nuclear explosion of 12 August 1953. The explosion yield was 400 kt. The calculations were performed for the radioactive particle transport from a linear vertical source with a height distribution of the activity in the form of a truncated Gaussian distribution. Particle size activity distribution is approximated by a lognormal law. In the calculations the distribution parameters are assumed to be the same as those of surface explosions for the Nevada coherent soils: $\lg \delta = 2.053$ and $\sigma = 0.732$ (Stewart, 1956). It is noteworthy that particle activity distribution parameters are related to the type of the soil of the underlying surface, and for the Semipalatinsk Test Site they do not differ much from those given above. Figure 4.37 gives the experimentally measured dose rates in the axis of the cloud pattern from the explosion of 12 August 1953, at 26 h after the explosion compared with the calculated values. Dose-rate distributions in the intermediate and remote zones are shown in Figure 4.38 in the form of isolevels of the dose rate logarithm according to the original data. The calculations show that a vast territory was contaminated by this explosion, including West Siberia and the southern part of the Altai Republic.

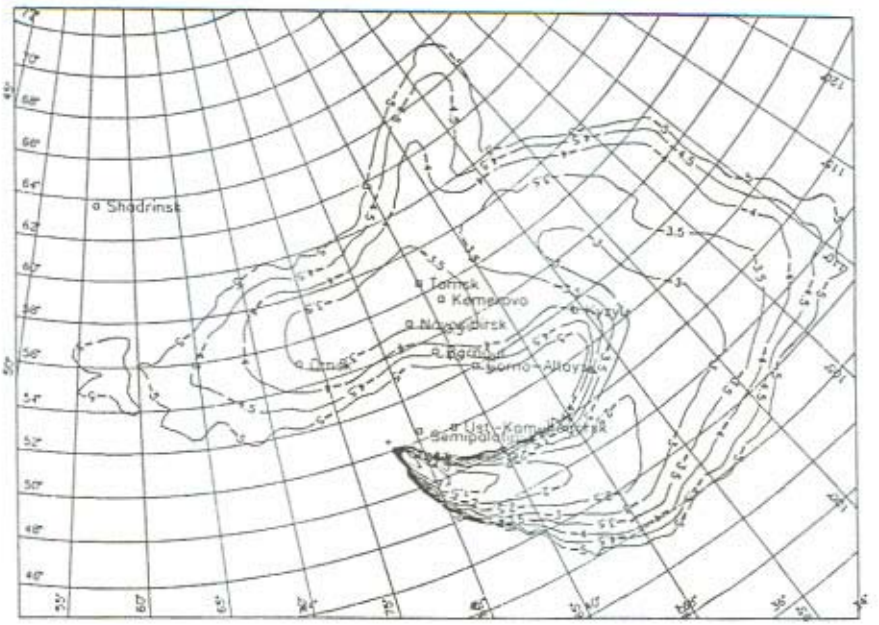

Figure 4.38 Calculated distribution of the dose rate in isolines logarithm isolevels in the intermediate and remote zones dose rate, R h^{-1} (85 mGy^{-1}).

4.5 RADIOACTIVE CONTAMINATION OF GEOLOGICAL FORMATIONS, UNDERGROUND WATER, GAS AND OIL BY UNDERGROUND NUCLEAR EXPLOSIONS

The problems of the underground water contamination from underground nuclear explosions, as well as the contamination of oil and gas where stimulated production is carried out with the help of nuclear explosions, were discussed by Izrael *et al.* (1971). In the broken rock surrounding an underground nuclear explosion, three typical zones can be identified: the initial spherical cavity, the collapsed rock column and an adjoining zone of fractured rock. The geometrical parameters of these zones can be calculated approximately using empirical formulae. The generalized configuration of the destruction zones and their approximate typical dimensions based on numerous studies are given in Figure 4.39 (Izrael *et al.*, 1971).

A spherical cavity is formed as a result of pressure forces in a high-temperature epicentral zone. At the moment cavity formation is over the pressure of the vapour and gases that fill the cavity is approximately equal to the lithostatic rock pressure at ground zero. As a result of the blast wave effect,

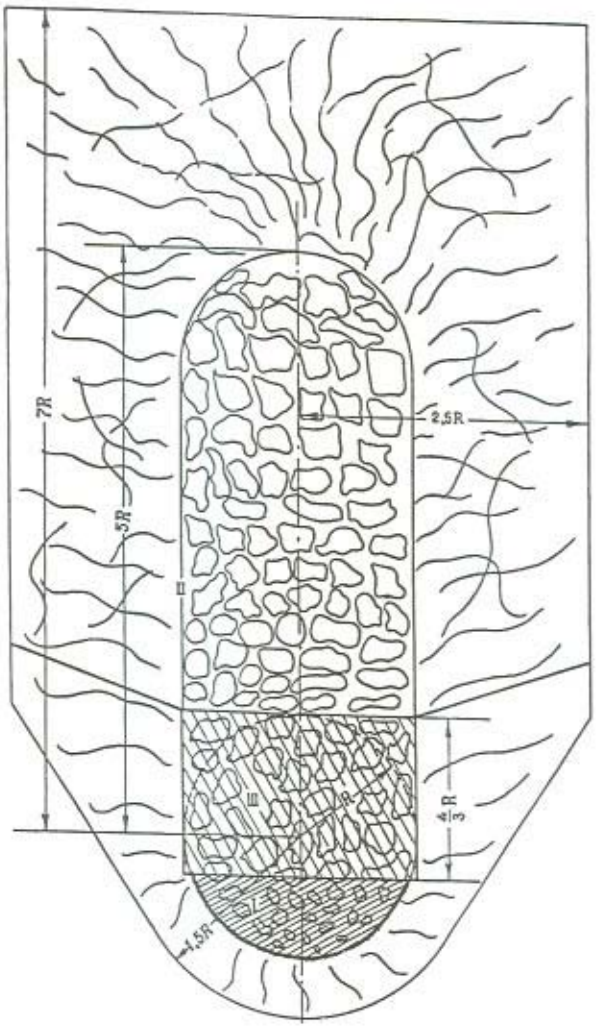

Figure 4.39 Configuration of zones of rock destruction in and around the cavity formed by a contained, underground nuclear explosion.

the zone of collapsed and fractured rocks spreads out around the spherical cavity. In the process of cavity cooling and condensation of the evaporated substances the pressure in the cavity drops. As a result the crushed and fractured upper rocks collapse and form a collapse 'column' or 'tube' (seldomly encountered in the exceptional circumstances of nuclear explosions in plastic rocks such as salt).

The specific nature of the radioactive contamination of all zones of the collapsed and fractured rock is much dependent on conditions at the moment the cavity collapses. Investigations have shown that most of non-volatile radioactive products are concentrated in the fused rock, which when falling in from the cavity walls form a lens in the lower third of the cavity and drag along the rocks that happen to fall into the melt before its solidification. The melt volume is below 5% of the cavity volume.

Gaseous radioactive products, e.g. radionuclides of inert gases as well as their decay products, remain in the cavity until its collapse, although a possible partial release of gas and volatile products through rock fractures cannot be excluded. The cavity collapse causes gases leaving the cavity to quickly fill the vacuum in the collapsed column zone. The fracture zone located outside the collapsed column is filled more slowly by the radioactive gases, because this requires an air exchange or displacement of the air in the fractures.

Radionuclides of inert gases (^{133}Xe and ^{85}Kr), of iodine (^{131}I and ^{133}I), tritium (^{3}H) and of radionuclides of gaseous precursors (^{89}Sr, ^{137}Cs, ^{90}Sr, ^{91}Y, ^{140}Ba) or volatile gases *per se* (^{132}Te, ^{103}Ru, ^{106}Ru, ^{125}Sb) are most important when spreading in broken rocks. Radionuclides of inert gases spread into the collapsed rock zone; if this zone is connected with the ground surface then a jet of inert radioactive gases can be formed in the atmosphere. Radionuclides ^{133}Xe and ^{85}Kr, and to some extent ^{135}Xe, are of greatest importance. Because of their high volatility, the radionuclides of iodine (particularly ^{131}I) are of significant importance as a potential source of contamination of the environment, at least during the first three months after the explosion. Most important for the contamination of broken rocks will be radionuclides of the inert gas decay products: ^{89}Sr, ^{137}Cs, ^{90}Sr + ^{90}Y, ^{91}Y and ^{140}Ba + ^{140}La, because the half-lives of the gaseous precursors of these radionuclides are comparable with the duration of the phases of formation of the 'collapse column'.

Figure 4.40 shows the relationship between the moment of collapse and the amount of radionuclides contaminating the column of collapsed rocks. Independent ^{235}U fission neutron yields are used for the calculation. The results are given in Ci of the *i*th radionuclide per kiloton of fission yield of nuclear explosion.

The maximum volume of zone II (Figure 4.39) is determined by the volume of the fractured rock (in this case the specific rock contamination must decrease with the distance from the centre), and the minimum value V_2 is determined by the volume of the chimney rubble. In this case the rock contamination can be close to uniform.

One more zone (III) must be mentioned (Figure 4.39). In this zone one can detect isotopes of elements that have chemical compounds which are volatile at relatively low temperatures; ^{132}Te + ^{132}I, ^{106}Ru + ^{106}Rh, ^{103}Ru and ^{125}Sb can be considered as typical representatives of this group of radionuclides.

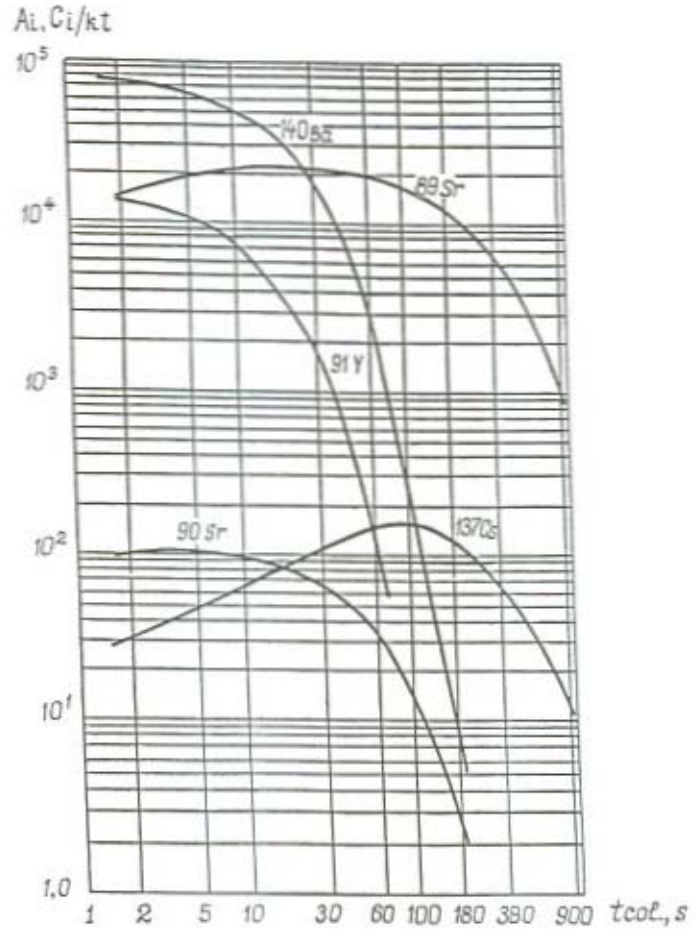

Figure 4.40 The relationship between the activity of various radionuclides contaminating the broken rocks and moment of cavity collapse (LCi = 37GBq).

The secondary processes of migration and post-explosion radionuclide redistribution are mainly linked to their solubility, i.e. to the ability of the radionuclide to transit from explosion products to water solutions. Most underground nuclear radioactive explosion products in the zone of the fragmented rocks are connected with the solidified melt and are not prone to leaching or scavenging. Rocks in the chimney rubble are mostly contaminated on the surface, and this definitely may promote the transfer of radionuclides to water solutions. The same applies to particles produced in cratering explosions. The extent to which radioactive products in a particle pass into the water is

variable: for example, particles with a volume activity distribution lose as a whole about 1–4% of the total activity to water.

The solubility data of the radionuclides are related to their gaseous precursor history; the most soluble radionuclides being those adsorbed on particle surfaces after the formation from their gaseous precursors. The solubility of radionuclides without gaseous precursors is very low. The relative solubility with respect to 1.0 for ^{90}Sr, is as follows (Izrael, 1974):

^{89}Sr	^{90}Sr	^{125}Sb	^{140}Ba	^{103}Ru	^{106}Ru	^{134}Cs, ^{137}Cs, ^{141}Ce	^{91}Y, ^{95}Zr, ^{144}Ce, ^{54}Mn, ^{60}Co
1.25	1.0	0.3	0.24	0.1	0.04	0.02	0.01 – 0.001

The redistribution or subsequent transport of the radioactive debris has been examined previously in the context of hydrological transport. During the year following the '1003' explosion, groundwater flowed into the crater to a total volume of about 500 m^3. Radiochemical studies of the water in the crater were undertaken to examine the way the crater filled and the role played by groundwater in creating artificial reservoirs. The major radionuclides observed were ^{89}Sr, ^{90}Sr, ^{103}Ru and ^{106}Ru. Also detected were ^{125}Sb and ^{137}Cs. It was noted that ^{90}Sr and ^{137}Cs were in cation form.

Groundwater transport of the radionuclides was studied with a network of observation holes established at the '1003' explosion site, at depths of 26 to 50 m, and located from 200 to 700 m from the emplacement hole (Izrael *et al.*, 1970a). Systematic hydrogeological observations were begun two months after the explosion. The authors noted that the crater shape was preserved during one year period and that the water levels in the holes were lowered by 0.7 to 1.3 m. They concluded that infiltration of groundwater into the crater occurred. Measurements in the observation holes confirmed the absence of radioactivity contamination in the holes even after several years following the explosion.

Consider the possibility of radionuclide migration with the underground water, outside. By writing down an ion exchange equation, the reaction constant can be determined and then the K_d, constant, which is referred to as a distribution factor. The letter indicates the relationship of bound ions in solid and in liquid phases. The K_d value changes within the range of 10^1–10^5 for different minerals and radionuclides. The mean K_d values are 10^2–10^3 for ruthenium, 10–2×10^4 (10^5 in some cases) for strontium, and 10^4–2×10^5 for cerium.

The average K_d value for a one-year mixture of fission products is estimated as 370. It is evident that $K_d = 0$ for tritium (Izrael, 1974). Thus the ion exchange processes lessen the potential hazard of underground water contamination, firstly due to decrease of ion transport velocity in comparison to the water flow velocity and secondly due to concentration decrease in migration. The flow velocity of a given substance (F_a) in the underground water can be expressed by the following formula:

$$F_a = F_b/(1 + \rho K_d) \quad (4.22)$$

where F_b is water flow velocity and K_d is the relation on mineral weight to water weight per volume unit of the given mineral and ρ is apparent density of porous medium/void fraction; usually K_d = 4–5. It follows from equation (4.22) that a given ion type velocity migrating with the water, flows at a rate 100 to 1000 times lower than the water flow velocity. For example, ^{90}Sr migration of 1 km distance will take years, even if F_b velocities are relatively high (about 10 m/day^{-1}).

Based on the above data, consider a specific case and assess possible oil contamination when stimulating oil production with nuclear explosions. It is known that the former USSR was first to use a contained nuclear explosion for stimulating oil production. For that purpose, on 30 March 1965, first two devices of 2.3 kt were exploded simultaneously in the oil block, then on 10 June 1965, one more device of 7.6 kt was exploded (Kedrovsky, 1970; Mikhailov *et al.*, 1996). A calculation model is described in detail by Izrael *et al.* (1971a). Here only the input parameters and results are considered.

Radioactive contamination by radionuclides with volatile precursors, such as ^{89}Sr, ^{90}Sr, ^{137}Cs, etc., was determined as a maximum assessment, i.e. with a uniform distribution of 40% of the above radionuclides produced by the explosion in the zone of chimney rubble and fracturing. It was assumed that operating holes were located in the fractured zone. The oil well discharge was assumed to be 30 t day^{-1}. The fractured zone volume in the calculation model considered is about 10^6 m^3, and at a mean rock porosity of about 18% (in the case considered it changed from 0.5 to 35%) and oil specific gravity of 0.86 g cm^{-3} (Kedrovsky, 1970), the specific oil content in the rock equals 0.15 g cm^{-3}. The coefficient of radionuclide transit into the oil was assumed to be equal to 10^{-3}–10^{2}, which is in a good agreement with values obtained in practice (Kedrovsky, 1971).

The calculated data (Tables 4.9 and 4.10) are confirmed experimentally by oil contamination values in the experimental explosion described (Kedrovsky, 1970, 1971).

The ^{137}Cs concentration, for example, in the oil from a hole at 40 m from ground zero, 2–4 years after the explosion, was below 10^{-9} Ci l^{-1} (37 Bq l^{-1}) (Kedrovsky, 1970).

Among all the applications that have been studied in the USA, the use of nuclear explosives for the stimulation of production from gas reservoirs is the closest to commercial utilization. Two field experiments have been conducted, projects 'Gasbuggy' and 'Rulison' and a number of other gas stimulation experiments are under preparation. 'Gasbuggy' was a 29 kt explosion carried out at a depth of 1292 m in December 1967. It provided the first data in the physical and chemical effects of a nuclear explosion in a gas reservoir. The changes in concentration of tritium and ^{85}Kr in the gas after explosion 'Gasbuggy' are reported by Nordyke (1971).

Table 4.9 The time that oil is delivered into observation holes at different distances from the source.

Distance	0.5 m	1 m	5 m	10 m	50 m
Time	0.6 day	2.5 days	52.5 days	250 days	17 years

Table 4.10 The ith radionuclide content in the oil $q_i(t)$ delivered into the oil at various time intervals, Ci l^{-1} (Bq l^{-1})

t	1 day	10 days	60 days	1 year	2 years	4 years
^{89}Sr	$4{\cdot}10^{-9}$ (147)	$5{\cdot}10^{-9}$ (185)	$4.4{\cdot}10^{-9}$ (163)	10^{-10} (3.7)	$8.5{\cdot}10^{-13}$ ($13.7\ 10^{-3}$)	$7{\cdot}10^{-15}$ ($2.6{\cdot}10^{-4}$)
^{137}Cs	$27{\cdot}10^{-11}$ (10)	$5{\cdot}10^{-11}$ (1.8)	$7.5{\cdot}10^{-10}$ (128)	10^{-10} (3.7)	$1.4{\cdot}10^{-10}$ (5.2)	$1.7{\cdot}10^{-10}$ (6.3)

4.6 ECOLOGICAL EFFECTS OF NUCLEAR TESTING

Ecological studies have been conducted at several nuclear explosion sites, which include sites of cratering experiments and sites used for testing nuclear weapons.

The effects of the testing programme at these sites cannot, in general, be ascribed solely to radiation, because of the concomitant effects of blast and heat. Furthermore, human exploitation of the natural resources in the test areas has changed markedly as a consequence of the testing programme. Although many significant and complex effects on ecosystems have been observed, the recovery processes following test explosions have been relatively rapid and vigorous. Deleterious effects on marine and terrestrial populations have not been persistent, presumably because of the rapid decline in the intensity of radiation and other impacts, the selective elimination of defective genetic information, and the recolonization of damaged areas with healthy individuals from distant localities (IAEA,1992).

4.6.1 Case study: Mururoa and Fangataufa

A summary is provided of the main results of the ecological studies performed by French scientists at the atolls of Mururoa and Fangataufa, which appears in the conclusions of the Volume III, *Le milieu vivant et son évolution* (Bablet *et al.*, 1995).

4.6.1.1 Consequences of the presence of the 'Centre d'Expérimentation du Pacifique (CEP)' on Terrestrial Flora and Fauna

In 1994, the terrestrial flora, which was destroyed or burnt by the effects of atmospheric tests, is little different from the original flora, both in diversity and

in size. However, on some mounds, those nearest to the oldest trials, the size of some plants (Guettarda and Scaevola) is smaller than in 1966. This is attributed to the degradation of the soil, already originally less fertile, by the thermal flash of atmospheric tests. Fangataufa sheltered, in 1966, numerous colonies of birds whose nest sites were spread all over the emerged crown. Their number, which was greatly diminished as a result of the direct effects of the size of the nuclear tests and the disappearance of their habitat, was restored after restoration of their habitat. In 1994, the population of birds was comparable to that in 1966. Meanwhile, species of small size have vanished, and the nests sites are now limited to the motu (mound) of the Pavillon sector. This reduction of the habitat was due to atmospheric tests, but also to the presence of humans and the civil engineering work, which drove the birds towards the most distant and least perturbed mounds. Eventually, the proliferation of the iron tree, *Casuarina equisetifolia*, with an arrangement of branches that does not allow the building of nests could explain the relative standstill of this situation. Experiments have been carried out on germinated nuts of coconut palm trees planted on the mounds nearest to high-energy atmospheric tests, in order to study the fate of vegetation under the conditions of extreme pressure, temperature and radiation. Those that survived do not show any residual anomalies. The consequences of radioactivity induced by the atmospheric tests have been very weak in comparison with the blast and thermal wave. Any after effects of radiobiological origin, that is to say generated by direct irradiation from the atmospheric tests or their fallout, has not been apparent, either in the realm of vegetation or animals.

The underground experiments carried out beneath the raised crown resulted in a compaction of soil around the surface ground zero points. In the south-west sector, where the high-energy shots were carried out, some mounds originally were very slightly raised, but are now immersed and this has caused the disappearance of terrestrial vegetation.

4.6.1.2 Consequences of the Presence of the CEP for the Marine Flora and Fauna

The thermal flash of megaton tests has destroyed a high proportion of superficial coral and mollusc populations, in particular those of the external plates and of the algal crest near the ground zero point of the tests. The whitening of certain surviving colonies, by the loss of their zooxanthellae, has been regularly observed up to the cessation of the atmospheric tests. The phenomenon has introduced a disequilibrium into the ecosystem comparable with that produced after the passage of a tropical cyclone or an abnormally hot summer period. Fifteen years after the end of atmospheric testing, the coral population of those external plates was restored, with a diversity and a rate of recovery comparable with those existing before the tests. The rapidity of this restoration is probably

explained by the weak degradation suffered by the substrates. The population of molluscs of these areas has also been re-established to levels comparable with those of 1966, except for *Tecarius grandinatus*, populations of which still remain scattered. The pressure waves induced by the atmospheric and underground tests in the lagoon have resulted in hard substrate degradation and some increase in the rate of sedimentation. From this perspective the underground events had a greater impact on account of their dispersion and the considerable pressure that they generate around the surface ground zero points.

The vitality of the coral communities of the Mururoa and Fangataufa atolls varies greatly from one site to another, from one biotope to another, as a function of the natural environmental conditions and past and present perturbations.

Overall, the recolonization of the coral is active, but the restoration of coral populations following the atmospheric tests is more advanced than in the much more recent underground tests, which have generated a greater degradation of the substrates. The populations often present a young character, with sometimes a dominance of pioneer species, indicating a community still badly structured. Locally, the bioconstructor organisms can strongly compete with substitution populations: soft algae, Zoantharia, Alcyonaria and Actiniaria. In a number of cases, such as the east sector of Mururoa near the base or the navigation routes, the appearance of certain substitution populations can be linked to urbanization or human presence.

On the coral constructions of these sectors, the appearance of populations of Palythoa has been noted since 1969, with the subsequent, often cyclic, development of Zoanthus and Rhodactis. A reduction follows in the species diversity of Madreporaria by elimination of a species that does not tolerate the rise in nutrients and suspended or sedimented materials. The echinoderms and algae offer good examples of the spatio-temporal variability of populations due to perturbations in the surroundings by nuclear experiments. Comparable demographic expansions can be seen in zones near urban waste. On these sites, the strongest densities observed sometimes are attributable to the large quantities of organic material dispersed in the environment. The opening of the Fangataufa passage and, to a lesser degree, the augmentation of exchanges of water with the ocean by the hoa from the southwest of Mururoa, should modify certain populations. This is already most apparent where plankton is concerned. The populations of molluscs of a more open Fangataufa lagoon should evolve towards greater specific diversities and reduction in the density of original dominant species. This tendency seems to be appearing but, taking into account the impact of the nuclear events, it is still too soon for confirmation.

4.6.2 Case study: Nevada Test Site

Extensive searches for ecological changes in contaminated areas have also been carried out at the Nevada Test Site. In most of these studies, however, the

contamination consisted principally of mixed fission products, and, except for the work reported by Rhoads and Platt, the more dramatic ecological effects were generally attributed to non-radiological perturbations. The best opportunities for searching for ecological effects from plutonium alone exist (in a number of areas) adjacent to the Nevada Test Site in areas used for 'safety shot' tests. These tests involved detonation by conventional explosives of plutonium in various containment configurations. Studies of small mammals and grazing cattle in these areas have failed to discover any evidence of radiogenic pathology. Varney and Rhoads have examined shrubs in areas assumed to have been contaminated primarily with plutonium. Although their data implied that such shrubs had increased frequencies of chromosomal aberrations to controls, the evidence was not conclusive (Hanson, 1980).

The development of the Plowshare programme and the execution of the SEDAN event stimulated detailed radioecological studies of long-lived radionuclides. The distribution of tritium in the SEDAN ejecta field, climatic effects on this distribution, and inventory data were described in this research: the integrated inventory of radionuclides in SEDAN ejecta indicated that tritium was the most abundant radionuclide on the basis of activity per surface unit. The biological significance of residual tritium at SEDAN crater was evaluated in plant and animal studies

4.6.3 China

In China, the Institute for Application of Atomic Energy, established in 1960 under the auspices of the Chinese Academy of Agricultural Sciences, conducted radioecological experiments to study the behaviour of fission products from fallout origin in crops and soils (Xu Shiming *et al.*, 1996). On-the-spot pot culture experiments on crop plants were performed in the proximal area of a low-altitude nuclear explosion. Other experiments were performed using the fallout collected in the area of nuclear explosion tests. The results show that the fallout (0.5% solubility) contributed a little to the internal contamination of crops via roots. Unfortunately, in most of those experiments, which appear to have been conducted in the 1960s, only measurements of total beta or gamma were carried out, therefore, the valuable information that can be derived from these experiments is limited.

4.6.4 Former USSR

The estimation of genetic effects caused by nuclear tests at the Semipalatinsk Test Site was presented during the II NATO-ARW, Barnaul (Shumny and Shevchenko, 1994). Recurring atmospheric nuclear explosions at this test site contaminated certain areas of Altai from 1949 through to 1962 by as much as 3 Gy, which is enough to cause genetic effects. Mutagenic effects of irradiation in

Altai can be evaluated very approximately by examining organisms that differ in the length of generative cycles and occupy different ecological niches. The succession of generations is accompanied by elimination of mutant variants, and so is an additional factor that prevents an easy analysis. Therefore it was urgent to uncover possible traces of exposures to ionizing radiation in the hereditary material of currently living organisms, among them plants and animals which (or whose ancestors) have ever been exposed to radioactive fallout from the Semipalatinsk nuclear tests. With that objective, the cytogenetic and some biochemical markers of exposure to radiation have been analysed in material from human residents, animal populations (Chironimids) and plant populations (Scotch pine) of the affected Altai areas.

4.6.4.1 Cytogenetic Monitoring of the Natural Populations of Chironomids

There has been a three-time monitoring of seven Chironomid populations of Altai monitored on three occasions in 1992–1993. In some of the regions investigated the dose of ionizing radiation peaked at 3 Gy after the 1949 explosion. Today, soil concentrations of ^{137}Cs near the lakes are two to three times as much as the global fallout background. Study of chromosome polymorphism in the populations of the two species of the Altai Chironomids (*C. tentans* and *C. balatonicus*) revealed wide chromosome polymorphism in all populations studied, both in the polluted regions and in the conventional control. The findings show a difference witnessed by 'bundles' of five to seven unique sequences not reported in any other populations ever studied, except in the Cheliabinsk populations, where the level of radioactivity still remains high. It is noteworthy, that both the Altai and the Cheliabinsk populations are 60–90 generations removed from those exposed to the explosions of 1947 and 1957, respectively. Part of the neutral or adaptive chromosomal anomalies induced by radiation can persist through many generations. The unique sequences therefore may be regarded as 'radiation records' induced in the Chironomid genome following the exposure to radiation, which have persisted for 60–90 generations.

4.6.4.2 Examination of Wild Populations of Plants

Analysis of genetic and cytogenetic parameters of higher plants in Altai populations exposed to ionizing radiations has been performed by a team of scientists from the Institute of Cytology and Genetics of the Siberian Division of the Russian Academy of Sciences and from the Institute of General Genetics of the Russian Academy of Sciences. The Scotch pine (*Pinus silvestris*) is a natural test system for assessing remote genetic hangovers of exposure to radiation. The mutational events induced in the vegetation by nuclear tests may be identified as differences between wild populations from polluted

regions and control regions, using a series of parameters, such as pollen fertility, seed production, germination of seedlings, number of cells with chromosomal aberrations in seedlings going through mitosis I, frequency of meiotic anomalies and polymorphism for seed storage proteins. On the whole, this study provides evidence that radioactive pollution of the regions has induced lower pollen viability and fertility, rendering more seeds unviable, giving rise to meiotic anomalies and raising concentrations of rare and null variants of storage protein in the seeds of wild populations of the Scotch pine.

4.6.4.3 Lichen–Reindeer–Human Foodchain

Radioecological peculiarities around the Novaya Zemlya (Russia) test site have been investigated by Ramzaev's team since 1961, with special emphasis on the lichen–reindeer–human foodchain. The studies show that the structure of the lichen could increase the adsorption surface to a value 20 to 100 times greater than in grasses; furthermore the concentration of ^{137}Cs in the thalle is 200 times greater than in the aqueous solution of ^{137}Cs. In the case of ^{90}Sr this factor is 20 times greater. Another interesting observation is that the absence of roots in lichens created the illusion that the radionuclides in soil are inaccessible: actually lichen possess special features in regard to this and in three months lichen can absorb caesium from soil 200 to 400 times more than grasses can. The degree of assimilation of ^{90}Sr from soil is almost the same as in grasses (0.1–0.3%). These peculiarities of lichen have created preconditions for heightened levels of radionuclides (especially ^{137}Cs) in the subsequent portions of the foodchain, such as in reindeer, whose principal fodder for seven to eight months is lichen (Ramzaev *et al.*, 1993).

REFERENCES

Andrushin, I. A., Chernyshev, A. K., Logachev, V. A., Mikhalikhina, L. A., Stepanov, Yu. S., Krasilov, G. A., Matuschenko, A. M., Dubasov, Yu. V. (1994) The modern interpretation of the data of air- and surface-radiation reconnaissance of the pattern from the first nuclear explosion in the USSR in 1949. *International Conference, Barnaul, Russia, September.*

Bablet, J. P., Gout, B. and Goutière, G. (1995) *Les Atolls de Mururoa et de Fantagaufa (Polynésie française), Vol. III. Le milieu vivant et son évolution.* Masson et DIRCEN, Paris.

Boltneva, L. I., Izrael, Yu. A., Nazarov, I. M. and Ionov, V.A. (1977) ^{137}Cs and ^{90}Sr global contamination and external exposure doses over the USSR territory. *Atomnaya Energiya*, **42**, 355 and 360. (In Russian.)

De Geer, L. E. (1996) *Chinese Atmospheric Nuclear Explosions from a Swedish Horizon. A Summary of Swedish Observations of Chinese Nuclear Test Explosions in the Atmosphere 1964–1980.* National Defence Research Establishment FOA.

Demidovich, B. P., Maron, I. A. and Shuvalova, E. L. (1967) *Numerical Methods of Analysis.* Nauka, Moscow. (In Russian.)

Doury, A. and Musa, C. (1996) *La Part Française dans les Essais Nucléaires Atmosphériques et leurs Conséquences*. No.5 SMSRB/DIR du 10.10.96.

Dunning, G. M. (1959) Fallout from nuclear tests at the Nevada Test Site. In: *Fallout from Nuclear Weapons Tests*, Vol. 3. pp. 2021–113. Joint Committee on Atomic Energy USA, Government Printing Office, Washington.

Freiling, E. C. (1961) Radionuclide fractionation in bomb debris. *Science*, **133**, 1991–1998.

Freiling, E. C. (1963) Theoretical basis for logarithmic correlation of fractionated radionuclide compositions. *Science*, **139**, 1058–1059.

Hanson, W. C. (ed.) DOE/TIC-22800 (1980) *Transuranic Elements in the Environment*. National Technical Information Service, U.S. Department of Commerce, Springfield, VA 22161.

Haywood, S. M. and Smith, J. (1990) *Assessment of the Potential Radiological Impact of Residual Contamination in the Maralinga and Emu Areas*. NRPB-R237, National Radiological Protection Board, Chilton, Oxfordshire.

Heft, R. E. *et al.* (1971) *Nuclear Technology*, **11** (3), 413.

IAEA (1992) *Effects of Ionizing Radiation on Plants and Animals at Levels Implied by Current Radiation Protection Standards*. Technical Report Series, No. 332, International Atomic Agency, Vienna.

IAEA (1996) *Radiological Conditions at the Bikini Atoll, Republic of the Marshall Islands: the Prospects for Resettlement*. Editing draft 13, International Atomic Energy Agency, Vienna.

Izrael, Yu. A. (1973) *Isotope Composition of Radioactive Fallout*. Hidrometeoizdat, Leningrad. (In Russian.)

Izrael, Yu. A (1974) *Peaceful Nuclear Explosions and Environment*. Hidrometeoizdat, Leningrad. (In Russian.)

Izrael, Yu. A. (1996) *Radioactive Fallout after Nuclear Explosions and Accidents*. Progress-pogoda, Sankt-Petersburg. (In Russian.)

Izrael, Yu. A., Petrov, V. N., Pressman, A. Ya., Rovinsky, F. Ya., Stukin, E. D. and Ter-Saakov, A. A. (1970a) *Radioactive Contamination of Natural Environments from Underground Nuclear Explosions and Prediction Methods*. Hidrometeoizdat, Leningrad. (In Russian.)

Izrael, Yu. A., Kazakov, Yu. E. and Ter-Saakov, A. A. (1970b) Peculiarities of the atmosphere and terrain contamination from single and multiple cratering underground explosions. In: *Peaceful Atomic Explosions*, pp. 103–132. Atomizdat, Moscow. (In Russian.)

Izrael, Yu. A., Pressman, A. Ya., Bataev, K. G. and Stukin, E. D. (1971) Spread of radioactive products in the fractured-rock zone resulting from a completely contained nuclear explosion and calculation of possible contamination of oil through the attempt to intensify extraction by means of nuclear explosions. In: *Peaceful Nuclear Explosions II. Proceedings of a Panel, Vienna, 18–22 January 1971*, pp. 283–293. International Atomic Energy Agency, Vienna.

Izrael, Yu. A., Vakulovsky, S. M., Vetrov, V. A., Petrov, V. N., Rovinsky, F. Ya. and Stukin, E. D. (1990) *Chernobyl: Radioactive Contamination of Natural Environments*. Hidrometeoizdat, Leningrad. (In Russian.)

Izrael, Yu. A., Tsaturov, Yu. S., Nazarov, I. M., Petrov, V. N., Stukin, E. D., Fridman, Sh. D., Kontarovich, A. F., Fedotkin, A. F. and Kertsman, V. M. (1994) Reconstruction of actual radioactive contamination pattern produced by accidents and nuclear tests. *Meteorologiya i Hidrologiya*, **8**, 5–18. (In Russian.)

Izrael, Yu. A., Volkov, A. S. and Kovalev, A. F. (1995) The terrain radioactive con-

tamination of the former Soviet Union from nuclear weapon tests at Novaya Zemlya in the fall 1961. *Meteorologiya i Hidrologiya*, **5**, 5–12. (In Russian.)

Kedrovsky, O. L. (1970) The application of contained nuclear explosions in industry. In: *Peaceful Nuclear Explosions. Proceedings of a Panel, Vienna, 2–6 March 1970*, pp. 163–185. International Atomic Energy Agency, Vienna.

Kedrovsky, O. L. (1971) Completely contained nuclear explosions as a means of stopping uncontrolled oil and gas flows. In: *Peaceful Nuclear Explosions II. Proceedings of a Panel, Vienna, 18–22 January 1971*, pp. 209–222. International Atomic Energy Agency, Vienna.

Kedrovsky, O. L., Ivanov, I. Ya., Myasnikov, K. V., Mangushev, K. I., Valentinov, Yu. A., Leonov, E. A., Musinov, V. I. and Dorodnov, V. F. (1970) Osnovnyje technicheskije aspecty ispol'zovanija podzemnyh jadernyh vzryvov v narodnom hozjaistve. In: *Peaceful Uses of Nuclear Explosions*, pp. 5–51. Atomizdat, Moscow. (In Russian.)

Klement, A. W. Jr. (ed.) (1965) *Radioactive Fallout from Nuclear Weapon Tests*. AECS Symposium Series, Nov. 1964. USAEC Division of Technical Information Extension, Oak Ridge, Tennessee, USA. Proceedings of the Second Conference, Germantown, Maryland (Nov. 3–6, 1964).

Krey, P. W. and Fried, R. E. (1965) Long-range fallout from Sedan. In: Klement, A. W. (ed.), Proceedings of the Second Conference, Germantown, Maryland (Nov. 3rd, 1964) AECS Symposium Series, Nov. 1965, pp. 82–97. USAEC Division of Technical Information Extension, Oak Ridge, Tennessee. *Radioactive Fallout from Nuclear Weapon Tests*.

Liu Ying and Zhu Changshou (1996) *Environmental contamination and health effects from iodine-131 in fallout in China*. Report RC.07.96, *SCOPE-RADTEST Workshop in Beijing, China*.

Loborev, V. M., Sudakov, V. V., Zelenov, V. I., Gabbasov, M. N., Markovtsev, A. S., Dyachenko, V. I. and Volobuev, N. M. (1994) Reconstruction of exposure doses of the population in the Altai Krai from the explosion of August 29, 1949. In: *Vestnik Nauchnoi Programmy 'Semipalatinsky Poligon—Altai'*, No. 1, pp. 27–56. (In Russian.)

Logachov, V. A. (1994) Features of an evaluation of radiation doses received by the population after atmospheric nuclear testing at the Semipalatinsk test site. *Assessing the Radiological Impact of Past Nuclear Activities and Events*, pp. 25–32. International Atomic Energy Agency, Vienna.

Logachov, V. A. (1996) Comparison of radiation doses to the population of the Russian Federation from atmospheric nuclear testing at the test sites of the former USSR and from the Chernobyl accident. *Report to the International Conference 'One Decade after Chernobyl: Summing up the Consequences of the Accident'*, Austria Center, Vienna, 8–12 April 1996. (In Russian.)

Mikhailov, V. V. (ed.) Andryshin, I. A., Bogdan, V. V., Vashchinkin, S. A., Zelentsov, S. A., Zolotukhin, G. E., Karimov, V. M., Kirichenko, V. V., Matushchenko, A. M., Silkin, Yu. A., Strukov, V. G., Kharitonov, K. V., Tchernyshev, A. K., Tsyrkov, G. A. and Shumaev, M. P. (1996) *USSR Nuclear Weapons Tests and Peaceful Nuclear Explosions, 1949 through 1990*. RFNC-VNIIEF, Sarov.

Nordyke, M. D. (1971) Underground engineering applications, concepts and experience: gas stimulation with PNE. In: *Peaceful Nuclear Explosions II. Proceedings of a Panel, Vienna, 18–22 January 1971*, pp. 23–59. International Atomic Energy Agency, Vienna.

Nordyke, M. D. and Wray, W. (1964) Cratering and radioactivity results from a nuclear cratering detonation in basalt. *Journal of Geophysical Research*, **69**, 675–689.

Norris, R. S., Barrous, A. S. and Fildhaus, R. V. (eds) (1994) *Reference-book on the*

Nuclear weapon. Annex 1. Vol. 5. The English, French and Chinese nuclear weapons. Council of the Defence of the Natural Resources.

Petrov, V. N. and Pressman, A. Ya. (1962) Otsenka vliyaniya turbulentnogo rasseyaniya po vertikali i v napravlenii vetra na rasprostranenie polidispersnoy primesi. Reports of Academy of Sciences of the USSR, **146**, 86–88. (In Russian.)

Ramzaev, P. V., Miretsky, G. I., Troitskaya, M. N. and Dudarev, A. A. (1993) Radio-ecological peculiarities around the Novaya Zemlya (USSR) atomic testing range. *International Journal of Radiation Hygiene*, **1**, 1–13.

Shummy, V. K. and Shevchenko, V. A. (1994) Estimation of the genetic effects caused by nuclear tests at the Semipalatinsk Test Site. *NATO/SCOPE-RADTEST Advanced Research Workshop*, Siberia, Russia, 5–10 September.

Stewart, K. (1956) The condensation of a vapour to an assembly of droplets or particles (with particular reference to atomic explosion debris). *Transactions of the Faraday Society*, **52** (2), 161–173.

US DOE (1994) *United States Nuclear Tests. July 1945 through September 1992*. DOE/NV-209 (Rev.14) December 1994, United States Department of Energy, Nevada.

Xu Shiming, Zhai Wenhu, Hou Lanxin and Shang Zhaorong (1996) The shifting and control measures of radionuclides of nuclear fission products in crops and soils. Paper presented at the *SCOPE RADTEST Workshop, Beijing, China*, 19–22 October.

Zheng Yi, Mao Yongze and Li Iiangcheu (1996) Long range atmospheric transportation and fallout of nuclear test radioactive debris. Report RC.03.96, *SCOPE-RADTEST Workshop in Beijing, China*.

Zhu Changshou, Liu Ying (1996) The consequences of radioactive fallout deposition from nuclear test and health evaluation. Report RC.08.96, *SCOPE-RADTEST Workshop in Beijing, China*.